ChemSusChem

Chemistry Europe
European Chemical Societies Publishing
ChemSusChem

RESEARCH ARTICLE

Solvent-, Ligand, and Additive-Free Sonogashira-Type C–C Coupling by Mechanochemical Extrusion with Chitin-Derived Catalysts

Oscar Trentin[1] | Daniel Ballesteros-Plata[2] | Giordano Rossi[1] | Enrique Rodríguez-Castellón[2] | Maurizio Selva[1] | Alvise Perosa[1] | Daily Rodríguez-Padrón[1,3]

[1]Department of Molecular Science and Nanosystems, Ca' Foscari University of Venice, Venezia Mestre, Italy | [2]Department of Inorganic Chemistry, Facultad de Ciencias, Instituto Interuniversitario de Investigación en Biorrefinerías I3B, Universidad de Málaga, Málaga, Spain | [3]Section of Chemistry for the Technology (ChemTech), Department of Industrial Engineering, University of Padova, Padova (PD), Italy

Correspondence: Alvise Perosa (alvise@unive.it) | Daily Rodríguez-Padrón (daily.rodriguezpadron@unipd.it)

Received: 15 October 2025 | **Revised:** 15 December 2025 | **Accepted:** 15 December 2025

Keywords: biomass valorization | extrusion | heterogeneous catalysis | mechanochemistry | sonogashira coupling

ABSTRACT

Mechanochemical extrusion provides a sustainable and efficient approach for the preparation of mono- and bimetallic palladium and copper catalysts supported on nitrogen-doped carbons. In this study, palladium and copper mono- and bimetallic catalysts were synthesized via solvent-free extrusion and thoroughly characterized by XRD, HRTEM, N_2 physisorption, and XPS, revealing uniformly dispersed nanoparticles with strong metal–support and metal–metal interactions. The catalysts were evaluated in the model Sonogashira coupling of iodobenzene with phenylacetylene under continuous mechanochemical extrusion. The bimetallic Pd-Cu system exhibited superior activity and selectivity, effectively suppressing side reactions, such as phenylacetylene dimerization. A comprehensive parametric study, as well as analyses of substrate extent and catalyst recyclability, highlighted the crucial role of mechanical energy in enabling these transformations. Moreover, the dimerization of phenylacetylene was separately investigated, providing further insight into the formation of the corresponding dimer. Overall, these results demonstrate the ability of extrusion to finely control catalyst properties, optimize catalyst-substrate interactions, and offer a sustainable, solvent-free route to high-performance heterogeneous catalysts suitable for continuous-flow applications.

1 | Introduction

Transition-metal-catalyzed cross-coupling reactions are crucial tools in organic synthesis, enabling the formation of carbon–carbon and carbon-heteroatom bonds with high precision and functional group tolerance [1–4]. Among them, the Sonogashira coupling, which forms aryl-alkyne bonds, remains a cornerstone in C(sp^2)-C(sp) bond formation, with wide applications in materials science, pharmaceuticals, and agrochemicals [5–9]. Despite significant advances in reaction engineering and catalyst design, the development of greener and more scalable protocols for this transformation remains a challenge, particularly with respect to catalyst recyclability and the avoidance of toxic or resource-intensive additives [9, 10]. In recent years, efforts to render this transformation more sustainable have increasingly turned toward solvent-free and low-waste methodologies [11–14]. In this context, mechanochemistry has been increasingly explored as a solvent-minimized, energy-efficient alternative for cross-coupling reactions [15–19].

For example, Ito and coworkers developed a high-temperature ball-milling protocol for the Sonogashira coupling of polyaromatic halides, offering access to materials-oriented alkynes in excellent yields and short reaction times [20]. This method for aryl bromides utilized palladium(II) acetate ($Pd(OAc)_2$, 10 mol%) in combination with XPhos (*2-dicyclohexylphosphino-2′, 4′, 6′-triisopropylbiphenyl*, 15 mol%) or triadamantylphosphine (Ad_3P, 15 mol%) as ligand and triethylamine (Et_3N) as the base: the reaction was carried out at 80°C for 60 min under liquid-assisted grinding conditions (LAG, 30 Hz) with water (η = 0.40 μL mg^{-1}) (Figure 1a).

For aryl chlorides, instead, $Pd(OAc)_2$ was used with BrettPhos (*2-dicyclohexylphosphino-3,6-dimethoxybiphenyl*) as the ligand, and 1,4-diazabicyclo [2.2.2]octane (DABCO) as the base (Figure 1b). Heating was achieved using a temperature-controlled heat gun placed above the milling jar. While the method shows a broad substrate scope, including poorly soluble polycyclic halides, scaling up such a setup was technically challenging due to external heating and the homogeneous nature of the catalytic system. Ito and coworkers also developed a high-temperature ball milling protocol for the Sonogashira coupling of polyaromatic halides, offering access to material-oriented alkynes in excellent yields and short reaction times [20].

Another mechanochemical protocol was developed by Borchardt and coworkers, who reported the Sonogashira coupling of aryl iodides using palladium milling balls as both catalyst and grinding medium (Figure 1c) [21]. In this system, cyclohexane ($\eta = 0.3\ \mu L\ mg^{-1}$), copper(I) iodide (CuI), DABCO, triphenylphosphine (PPh_3), and potassium carbonate (K_2CO_3) were used. Despite its originality, the approach raised questions on the reusability and cost of palladium metal as a milling material, particularly for scale-up. Recently, electromagnetic milling (EMM) has emerged as another mechanochemical approach. Unlike traditional ball mills, EMM uses ferromagnetic particles agitated by a rotating electromagnetic field. This technique has been applied to the Sonogashira coupling of aryl bromides using $Pd(OAc)_2$, CuI, PPh_3, K_2CO_3, and DABCO, showing promising activity under solvent-free conditions (Figure 1d) [22].

Unlike batch ball milling processes, twin-screw extrusion (TSE) is a continuous-flow mechanochemical technology, able to integrate precise temperature control, adjustable residence times, and high material yields [15, 18, 24–28]. These features make TSE suitable for scalable, solvent-minimized synthesis [15, 29–31]. However, to date, extrusion has had limited application in Sonogashira chemistry. To the best of our knowledge, the only reported case was developed by Hastings and collaborators, who used a copper/palladium system [$Pd(OAc)_2$, CuI, PPh_3] for the cross-coupling of pyrazine derivatives, with K_2CO_3 as a base at 115°C and 100 rpm (Figure 1e) [23].

All these mechanochemical strategies for Sonogashira coupling present a common significant limitation due to the use of precious metal-based homogeneous catalytic systems including external ligands that can hardly be recovered or recycled. This is not only a bottleneck for downstream processing but also compromises the sustainability of the overall process.

Our group has recently demonstrated the versatility of extrusion for diverse applications, including the synthesis of heterogeneous catalysts, the oxidation of solid substrates such as vanillyl alcohol, and cross-coupling reactions such as the Suzuki-Miyaura reaction under additive-free conditions [17, 18, 32]. These advances showcased extrusion as a green and scalable platform for complex chemical transformations. We wish to report here a further development of this concept based on the design of an original and novel protocol for the Sonogashira reaction using ligand-free, heterogeneous catalysts prepared from renewable feedstocks. The catalysts, based on Pd and Cu, either mono- or bimetallic, have been synthesized through extrusion using chitin as the nitrogen and carbon precursor. These materials enabled efficient cross-coupling without the need for external ligands or additives and can be recovered and reused without significant loss of activity (Figure 1f). This study also provided insight into phenylacetylene dimerization as a parallel reaction pathway under extrusion conditions [33]. Overall, this work contributed to the development of more sustainable and scalable cross-coupling methodologies, leveraging both green catalyst design and process intensification.

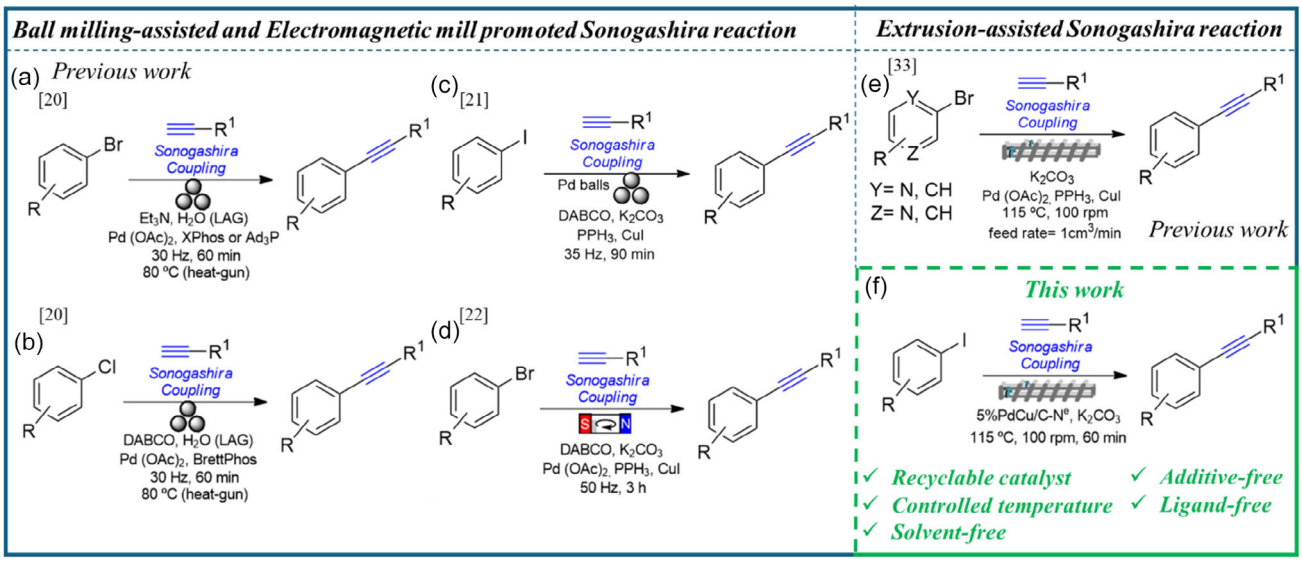

FIGURE 1 | State-of-the-art on mechanochemically assisted Sonogashira coupling. (a,b) High-temperature ball-milling protocol for the Sonogashira coupling of polyaromatic halides, developed by Ito and coworkers [20]. (c) Sonogashira coupling of aryl iodides using palladium milling balls as both catalyst and grinding medium, reported by Borchardt and coworkers [21]. (d) Sonogashira coupling of aryl bromides under EMM, developed by Zhang and coworkers [22]. (e) Sonogashira coupling of pyrazine derivatives under mechanochemical extrusion, reported by Hasting and coworkers [23]. (f) This work, Sonogashira coupling under mechanochemical extrusion, using heterogeneous chitin-based catalyst, without any additives, solvents, or ligands.

2 | Results and Discussion

2.1 | Synthesis and Characterization of Catalysts

The preparation of chitin-derived mono and bimetallic heterogeneous catalytic systems by extrusion represents a novel and sustainable approach. This continuous, solvent-minimized mechanochemical process has enabled the generation of robust materials with well-dispersed active sites, while simultaneously valorizing a renewable biopolymer as support [34–37]. In this contribution, the catalytic materials were mainly prepared by extrusion with metal contents ranging from 1 to 5 wt%, adapting a protocol previously reported by our group. These catalysts were compared with analogs obtained through conventional methods (solution-based and impregnation strategies) [34]. The samples made by extrusion were labeled as 5%PdCu/C–N^e, 5%Cu/C–N^e, 5%Pd/C–N^e, and 1%Pd/C–N^e (Figure 2), while the samples prepared by impregnation and solution-based methods were denoted as 5%Pd/C–N^i and 5%Pd/C–N^s, respectively.

Comprehensive multitechnique structural and surface characterization confirmed the tailored physicochemical properties. The following section examines the structural features of the catalysts, their activity and selectivity in C—C bond formation, and the crucial interplay between composition, structure, and performance.

2.1.1 | X-Ray Diffraction (XRD) Analysis

The crystalline structure and arrangement of the materials synthesized via extrusion were investigated by XRD, with the corresponding diffractograms shown in Figure 3. XRD patterns of other samples prepared by impregnation and solution methods have been reported previously by our research group [17]. A full description of all diffraction features of the extruded materials is provided in the Supporting Information. Overall, all XRD patterns exhibited consistent features. The diffraction peaks at 39.9°, 46.5°, and 67.9° corresponded to the (111), (200), and (220) planes of metallic Pd(0), consistent with a face-centered cubic structure [38]. As expected, these reflections were more pronounced in the 5 wt% Pd samples than in the 1 wt% Pd samples (see Figure 3). In the Cu-containing samples, two copper species were identified: metallic Cu, evidenced by diffraction peaks at 44.2° and 50.2° corresponding to the (111) and (200) planes, and Cu_2O, as indicated by the peak at 43.1° assigned to the (200) plane. These peaks were clearly observed in the 5%Cu/C–N^e sample [39–42].

The same reflections from Pd and Cu species were also observed in the 5%PdCu/C–N^e bimetallic catalyst, albeit with reduced intensity, thereby confirming the coexistence of Pd and Cu phases. The relative peak intensities and widths suggested the presence

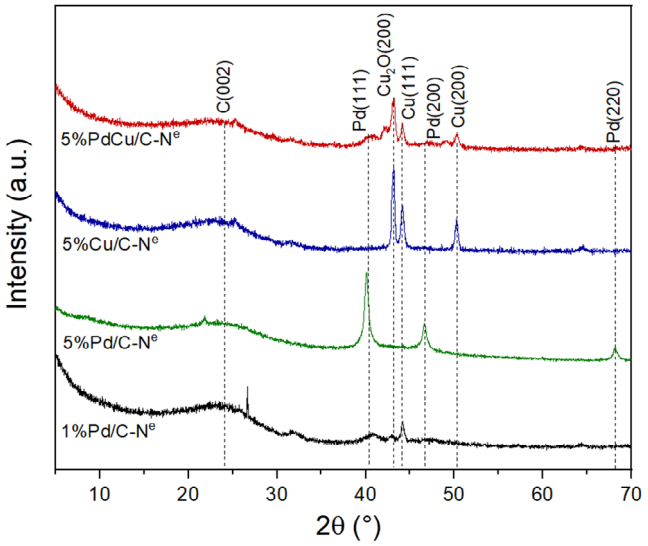

FIGURE 3 | XRD pattern of 5%PdCu/C–N^e, 5%Cu/C–N^e, 5%Pd/C–N^e, and 1%Pd/C–N^e.

of small Pd-Cu crystallites, consistent with the formation of nanoscale bimetallic regions [43, 44]. The broader diffraction peaks observed for the bimetallic Pd-Cu system, despite comparable particle sizes, particularly for the Pd nanoparticles (as discussed later in the microscopy section), could be ascribed to microstrain effects arising from lattice distortions and compositional heterogeneity induced by alloy formation. In addition, shoulder feature at ca. 42.1°, located between the Pd(111) reflection (39.9°) and the Cu_2O(200) and Cu(111) reflections (43.1° and 44.2°, respectively). This shoulder most likely originated from the partial overlap of Pd and Cu contributions, further shifted by lattice distortions due to alloying [44]. Such asymmetry in the diffraction profile indicated that the 5%PdCu/C–N^e catalyst was not a perfectly homogeneous alloy but contained regions of different local composition, where Pd-rich, Cu-rich, and oxide domains coexisted together with alloyed crystallites.

2.1.2 | N_2 Physisorption

The textural properties of the catalysts, including surface area, pore volume, and pore size distribution, were investigated by N_2 adsorption–desorption measurements at −196°C. All materials exhibited type IV isotherms with II-type hysteresis loops, characteristic of mesoporous solids (Figure 4 and Figure S1). Surface areas were determined using the Brunauer–Emmett-Teller (BET) equation, while pore volume and average pore diameter were calculated according to the Barrett–Joyner–Halenda (BJH) method [45, 46]. The extruded catalysts 1%Pd/C–N^e,

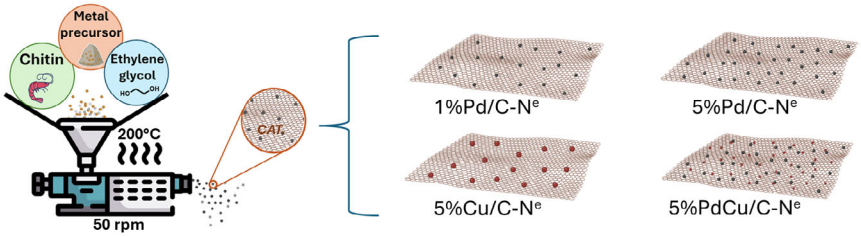

FIGURE 2 | Schematic representation of synthesis of catalytic materials through a mechanochemical-assisted approach.

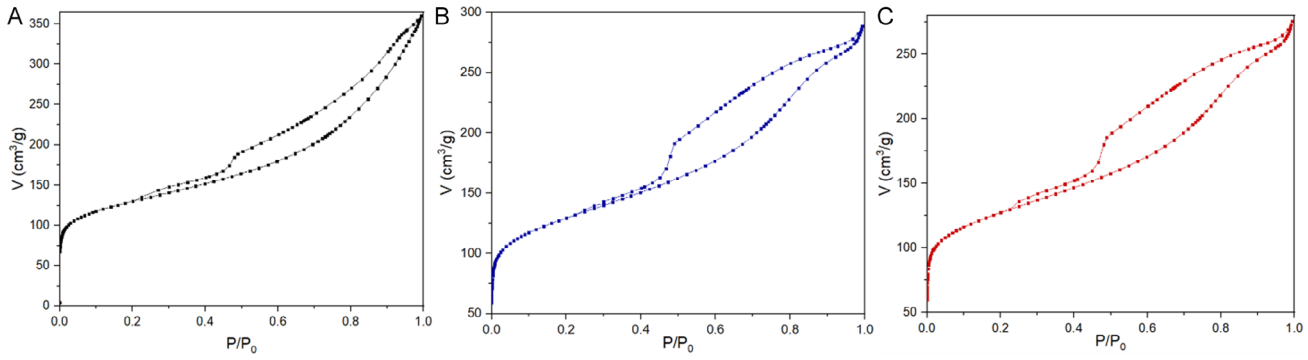

FIGURE 4 | Representative N_2 physisorption isotherms at −196°C of catalytic systems (A) 1%Pd/C–N^e, (B) 5%Cu/C–N^e, and (C) 5%PdCu/C–N^e.

5%Pd/C–N^e, 5%Cu/C–N^e, and 5%PdCu/C–N^e displayed high surface areas of 466, 498, 464, and 460 m^2g^{-1}, respectively, highlighting the favorable textural properties imparted by the extrusion method (Table S1).

These observations agree with our previous results, where a surface area of 321 m^2g^{-1} was measured for metal-free *N*-doped carbons derived from chitin [34, 47]. The incorporation of metal nanoparticles did not adversely affect the textural properties of the catalysts. Indeed, the incorporation of Pd and Cu was found to increase the surface area compared to their metal-free counterpart. Recent studies suggest that Pd nanoparticles on graphene-like supports could induce nanohole formation in carbon sheets, thereby enhancing the overall surface area and textural properties [48]. Moreover, the use of extrusion protocols further improved the surface area compared to analogous materials prepared via conventional solution-based or impregnation methods (See Table S1). Mechanical forces applied during extrusion could induce defects, edge sites, and partial exfoliation in the carbon matrix, contributing to the superior textural properties of the extruded catalysts [18, 49–52].

The average pore diameter of approximately 4.0 nm confirmed the mesoporous character of the obtained solids (Table S1). A slightly larger pore size (4.9 nm) was observed for the 5%Pd/C–N^e material, suggesting that both palladium loading and the extrusion process could contribute to an widening of the pore network. In contrast, the bimetallic systems displayed a slight reduction in pore size (3.4 nm). This effect was rationalized by the higher overall metal content (Pd + Cu), which tended to occupy or block part of the porous structure, together with the smaller particle size of the bimetallic domains. The latter may enhance the likelihood of partial pore occlusion, especially in the narrower regions of the mesoporous framework. A comparable trend was found for pore volume: the extruded samples exhibited values around 0.49 m^3g^{-1}, increasing modestly to 0.61 m^3g^{-1} for the 5% Pd/C–N^e material, while decreasing to 0.39 m^3g^{-1} in the bimetallic system. These results highlighted how the balance between metal loading, particle size, and synthetic method significantly influenced the textural properties of the materials.

2.1.3 | X-Ray Photoelectron Spectroscopy (XPS) Analysis

The surface chemical composition of the catalysts was investigated by XPS, and the corresponding spectra are reported in Figure 5. In the main text, we report only the Pd 3*d* and Cu 2*p* regions, as these are directly relevant to the catalytic behavior; the full XPS data set, including all additional regions, is provided in the Supporting Information. The deconvolution analysis of the high-resolution Pd 3*d* core level spectra provided detailed insights into the chemical states of palladium species present on the catalyst surface (Figure 5). For the 5%PdCu/C–N^e and 1%Pd/C–N^e samples, the spectra revealed four main components: peaks at (335.6 ± 0.2) and (340.8 ± 0.2) eV corresponded to the doublet Pd $3d_{5/2}$ – Pd $3d_{3/2}$ of metallic Pd(0), and additional peaks at (338.3 ± 0.2) and (343.9 ± 0.2) eV that were associated with the doublet Pd $3d_{5/2}$ – Pd $3d_{3/2}$ states of palladium bound to nitrogen [53]. The latter contributions suggested strong electronic interactions between Pd nanoparticles and the pyridinic/pyrrolic nitrogen functionalities of the carbon support, which are known to act as anchoring sites [54, 55].

By contrast, the 5%Pd/C–N^e sample exhibited not only the aforementioned Pd(0) and Pd-N components but also additional signals at (336.2 ± 0.2) and (341.5 ± 0.2) eV (Figure S2). These features were consistent with the presence of Pd(II) species,

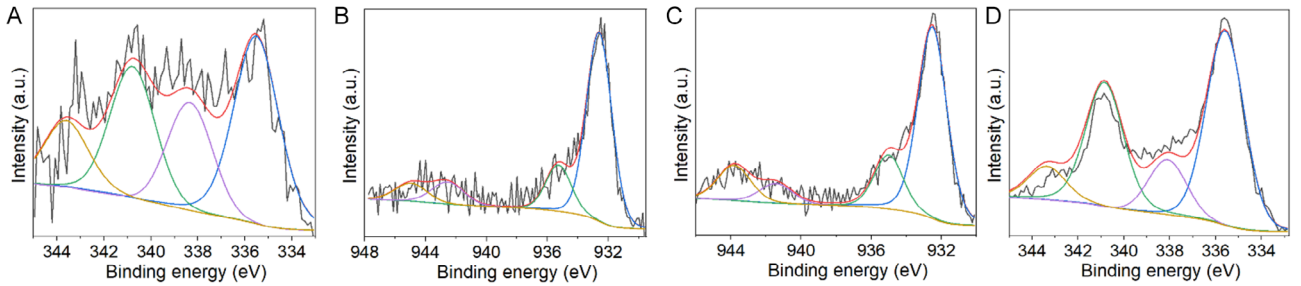

FIGURE 5 | High resolution XPS spectra of Pd 3*d* region of 1%Pd/C–N^e (A), region Cu 2*p* region of 5%Cu/C–N^e (B), Cu 2*p* region of 5%PdCu/C–N^e (C), and Pd 3*d* region of 5%PdCu/C–N^e (D).

most likely in the form of surface palladium oxide. The occurrence of Pd(II) in this material was rationalized by considering two factors. First, the higher Pd loading relative to the 1%Pd/C–N^e sample could reduce the extent of Pd-N coordination, leaving more exposed Pd atoms prone to oxidation. Second, the absence of Cu in 5%Pd/C–N^e removed the possibility of electronic and geometric stabilization effects provided by the Pd-Cu interaction. In the Pd-Cu bimetallic catalyst, copper could play a protective role by altering the electronic density of palladium and/or by preferential surface segregation, thereby mitigating Pd oxidation. Taken together, these results indicated that both the nitrogen content of the support and the presence of copper significantly influenced the oxidation state distribution of Pd, with stronger Pd-N coordination and Pd-Cu interactions favoring the stabilization of metallic palladium over oxidized species [56–58].

Finally, for the 5%Cu/C–N^e and 5%PdCu/C–N^e samples (Figure 5), the high-resolution Cu $2p_{3/2}$ core level spectra, registered with a low irradiation time, present a main contribution at (932.4 ± 0.2) eV, associated typically with both metallic Cu and Cu(I) species [59]. A weaker signal at (935.0 ± 0.2) eV was also observed, characteristic of Cu(II) species, most likely attributable to surface CuO. Moreover, weak satellites around (941.0 ± 1.0) and (944.0 ± 1.0) eV further confirmed the presence of Cu(II). Overall, the coexistence of metallic Cu and Cu_2O was consistent with the XRD results, whereas the additional detection of CuO suggests further surface oxidation of copper relative to the bulk material [42].

2.1.4 | High-Resolution Transmission Electron Microscopy (HRTEM) and Scanning Transmission Electron Microscopy–Energy Dispersive X-Ray Spectroscopy (STEM-EDX)

The morphological properties of the samples were further examined by HRTEM and STEM-EDX mapping (Figures 6, 7 and Figures S3, S4). Figure 6 presents the TEM micrographs of 1%Pd/C–N^e, 5%Cu/C–N^e, and 5%PdCu/C–N^e, while a representative TEM image of the 5%Pd/C–N^e sample is provided in Figure S3. In all cases, quasi-spherical nanoparticles with homogeneous morphology and uniform dispersion within the layered carbonaceous matrix were observed.

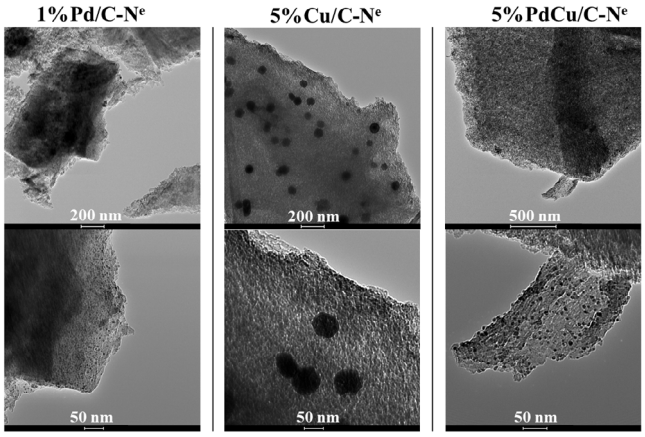

FIGURE 6 | Representative HRTEM of 1%Pd/C–N^e, 5%Cu/C–N^e, and 5%PdCu/C–N^e.

The mean particle size of the Pd nanoparticles was ≈14.9 nm for the 5%Pd/C–N^e sample, whereas slightly smaller Pd particles were obtained for the 1%Pd/C–N^e (8.3 nm) and 5%PdCu/C–N^e (9.1 nm) (Figures S4, S7). As discussed in the previous sections, this smaller size was attributed either to the lower Pd loading, which favors stronger coordination of Pd species with nitrogen atoms on the carbon support, or to the presence of copper, which can promote alloying effects and limit Pd particle growth [60, 61].

In the case of copper, a significant decrease in particle size was also observed, from ca. 24.5 nm with a broad size distribution in the monometallic Cu sample to 7.3 nm with a narrower distribution in the Pd-Cu bimetallic system (Figures S4, S7). This finding suggested that the simultaneous presence of Pd exerted a stabilizing effect, preventing extensive Cu nanoparticle growth [60].

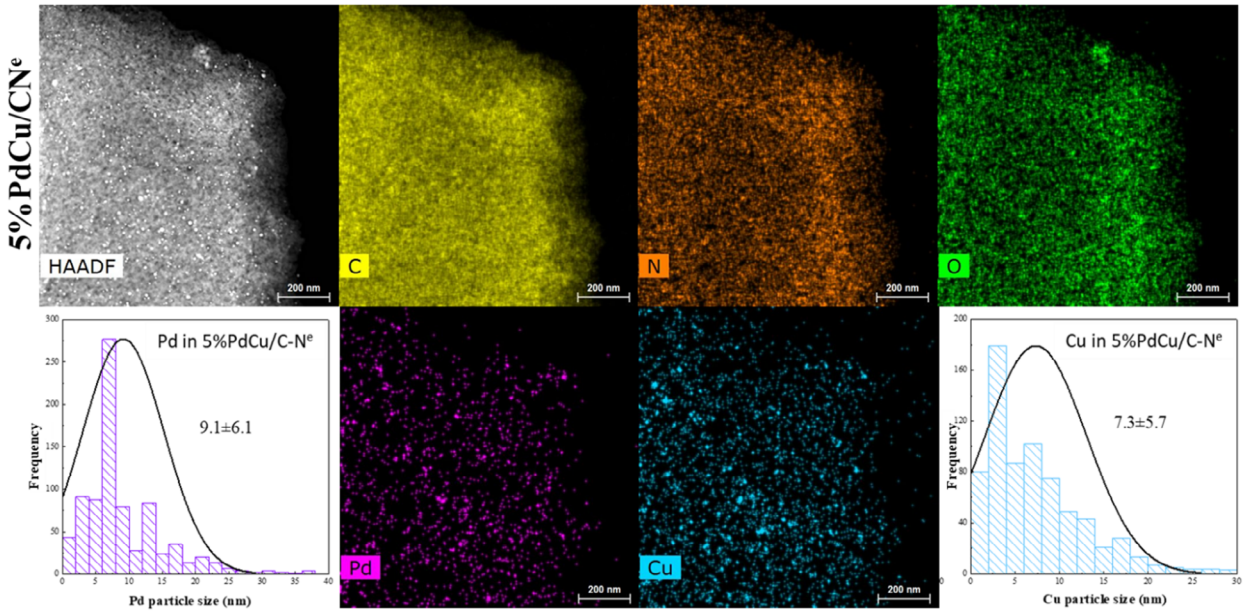

FIGURE 7 | STEM and EDX-mapping micrographs of 5%PdCu/C–N^e, with the corresponding Pd and Cu nanoparticle size distribution.

Finally, STEM-EDX mapping confirmed the homogeneous distribution of Pd, Cu, C, N, and O across the material.

2.2 | Catalytic Activity

The catalysts prepared by extrusion were evaluated in the Sonogashira coupling of iodobenzene and phenylacetylene. Palladium is the most effective metal for cross-coupling reactions, thanks to its ability to cycle reversibly between the 0 and 2+ oxidation states under relatively mild conditions [62–66]. However, in the specific case of the Sonogashira reaction, a cocatalyst, typically Cu(I), is often required to activate the terminal alkyne and facilitate the transmetallation step [67–69]. The accepted classical mechanism begins with the oxidative addition of the aryl halide to Pd(0), generating a Pd(II) intermediate. This is followed by transmetallation, where the alkyne, activated via coordination with the copper cocatalyst, undergoes nucleophilic substitution at the Pd(II) center. A final reductive elimination step then forms the new C—C bond between the sp-hybridized carbon of the alkyne and the sp^2 carbon of the aryl group, yielding the Sonogashira product (referred to as product **1,** Scheme 1), along with regeneration of the Pd(0) species. Concurrently, a base assists to the regeneration of the active Cu(I) species [70].

Competing side reactions may also occur: i) product **1** can undergo further addition with a second equivalent of phenylacetylene, leading to product **2** (Scheme 1) [5, 71–73]; ii) iodobenzene can undergo homocoupling, forming biphenyl (product **3,** Scheme 1) [74, 75]; and iii) terminal alkynes may dimerize (leading to the formation of product **4**, Scheme 1) or trimerize via metal-catalyzed pathways, further complicating product distribution [76, 77]. In literature, there are cases where product **1** interacts with a second iodobenzene to form a new C—C bond, although, as further discussed, this product was not observed under the mechanochemical conditions tested herein [78].

Experiments confirmed the formation of products **1**-**4** whose structures were validated by GC/MS and NMR analyses (details are in the Supporting Information section, Figures S8–S30).

The conversion and the cross-coupling selectivity (S_{cc}, %) were calculated with respect to the limiting reagent (iodobenzene) and the products **1**, **2** and **3**, respectively. In particular, the $S_{cc\text{-}i}$ selectivity towards product i ($i = 1$, 2 and 3) was defined according to the following expression

$$S_{cc-i} = [\text{mol } i / \text{conv. iodobenzene}] \times 100$$

where mol i was the total moles of compound i (determined by GC calibration), and conv. iodobenzene was the total moles of iodobenzene consumed in the cross-coupling reactions (Scheme 1, top).

However, to consider the formation of compound **4** that derived from the competitive dimerization of the excess reactant (phenylacetylene), the product distribution (PD, %) was introduced as another reaction metric to describe the relative amounts of all different products detected in the reaction mixture. Accordingly, PD_n for product n was defined

$$PD_n = [\text{mol } n / \text{mol } (\mathbf{1}+\mathbf{2}+\mathbf{3}+\mathbf{4})] \times 100$$

where mol n was the moles of compound n (determined by GC calibration), and mol (**1** + **2** + **3** + **4**) was the total moles of all observed products from both the cross-coupling reactions and the phenylacetylene dimerization (Scheme 1, bottom). To avoid redundant information and to immediately visualize the preferred reaction pathway, the iodobenzene-coupling to phenylacetylene-dimerization ratio (I/P, %) was calculated based on the PD_n values. This parameter was obtained by summing the PD_n contributions of all iodobenzene-coupling products (**1**, **2**, and **3**, for the component I, %) and those corresponding to phenylacetylene-dimerization (**4**, and, if present, **5** and **6**, for the component P, %). The resulting data are presented as stacked bar charts shown throughout the manuscript.

2.3 | Catalyst Screening

The Sonogashira cross-coupling reaction between iodobenzene and phenylacetylene was performed under solvent-free mechanochemical conditions using a twin-screw extruder. A preliminary catalyst screening was carried out to evaluate the performance of the synthesized materials compared with the commercial 5% Pd/C catalyst (Figure 8A,B). In all cases, the 5%Cu/C–N^e material was used as a cocatalyst. The extruder was charged with a manually premixed paste consisting of iodobenzene (5 mmol, 548 μL), phenylacetylene (1.5 equiv., 778 μL), K_2CO_3 (3 equiv., 2.1 g),

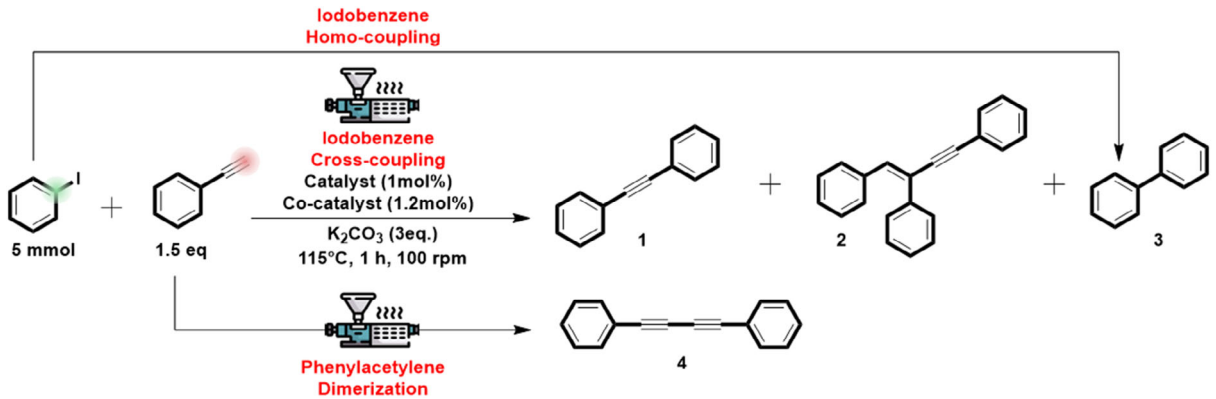

SCHEME 1 | Iodobenzene coupling (Sonogashira cross-coupling and homo-coupling) under reactive extrusion conditions, and phenylacetylene dimerization side-reaction.

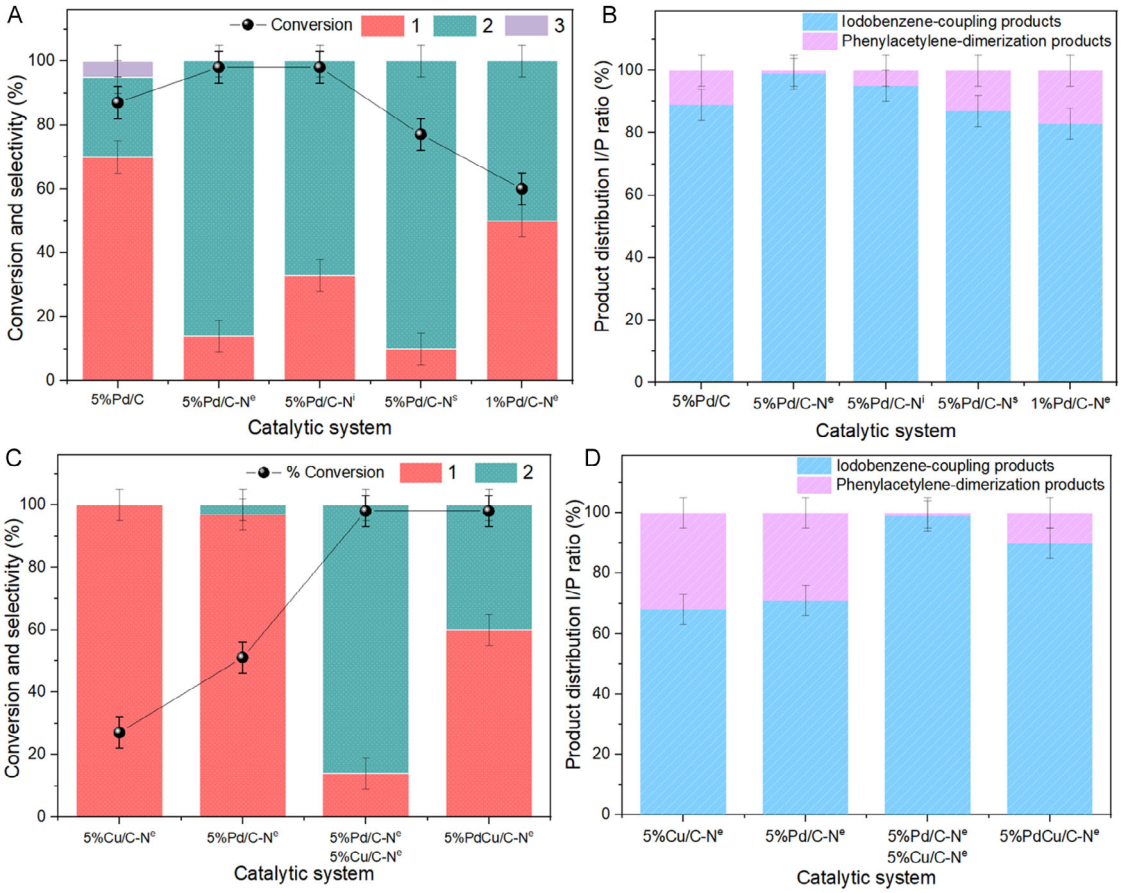

FIGURE 8 | (A,B) Catalyst screening of Sonogashira reaction. (C,D) Influence of cocatalyst and synergistic effect study. A–D: iodobenzene (5 mmol), phenylacetylene (1.5 eq.), K_2CO_3 (3 eq.), catalyst (1 mol%), 5%Cu/C–N^e (1.2 mol%), 115°C, 1 h, 100 rpm.

catalyst (1 mol%, 100 mg), and cocatalyst (1.2 mol%, 120 mg). The reaction was conducted for 1 h at 115°C with a screw rotation speed of 100 rpm based on the conditions reported by Hastings et al. [23].

As shown in Figure 8A, the highest iodobenzene conversions were achieved with the 5%Pd/C–N^e and 5%Pd/C–N^i catalytic materials (98% in both cases). These catalysts exhibited higher activity than the commercial 5%Pd/C reference (87% conversion) and, along with the formation of **1**, also promoted its further transformation into product **2** (selectivity towards **2** was 86% and 67% for 5%Pd/C–N^e and 5%Pd/C–N^i, respectively). Notably, only the commercial 5%Pd/C catalyst led to biphenyl formation (product **3**). This suggested that a nitrogen-doped support such as the chitin-derived one was effective in suppressing iodobenzene homocoupling. Interestingly, the 5%Pd/C–N^s catalyst showed a significantly lower conversion (77%) albeit with the highest selectivity for product **2** (91%). We assumed that the smaller Pd nanoparticles generated during the synthesis of this material interacted more strongly with the support enriched in pyridinic and pyrrolic nitrogen functionalities. These groups could act as *p*-type dopants able to withdraw electron density from the Pd nanoparticles, which thus became less nucleophilic and less active for the oxidative addition of iodobenzene. This hypothesis was supported by our previous study, in which charge density redistribution was analyzed via Kelvin Probe Force Microscopy (KPFM) [17, 79]. Additionally, once product **1** was formed, the occurrence of alkyne–alkyne coupling with phenylacetylene led to the formation of product **2** and impacted overall selectivity. Notably, while there is limited literature on tandem Sonogashira and alkyne–alkyne coupling reactions leading to product **2**, the solvent-free mechanochemical catalytic system developed in this study appeared well-suited for this transformation.

For the 1%Pd/C–N^e catalyst, although good selectivity toward product **1** was observed, the lower number of active sites limited iodobenzene conversion to approximately 60%. Nevertheless, under these conditions, the productivity of this material toward **1** was higher than that of the 5%Pd counterpart, resulting in overall good productivity levels (1.5 mol g_{Pd}^{-1} h^{-1}). Under these conditions, phenylacetylene dimerization became more competitive, resulting in the formation of up to 17% dimerization byproducts.

To assess the role of the cocatalyst, the activity of 5%Pd/C–N^e and 5%Cu/C–N^e was tested separately and compared with that of a physical mixture of the two catalysts and with the 5%PdCu/C–N^e bimetallic material (Figure 8C,D) under the conditions of Figure 8A. The bimetallic 5%PdCu/C–N^e catalyst and the mechanical mixture allowed near-quantitative conversion (98%) whereas the monometallic 5%Cu/C–N^e and 5%Pd/C–N^e catalysts achieved conversions of 27% and 51%, respectively. The sum of the activities of the separate catalysts was lower than that of the bimetallic 5%PdCu/C–N^e catalyst and of the mechanical mixture, indicating a synergy between Pd and Cu [80–84]. To further confirm Pd-Cu cooperative effects, the

theoretical catalytic performance of both the mechanical mixture and the alloyed bimetallic system was estimated as the additive contribution of the individual monometallic catalysts relative to the bare support (see Equations. S1, S2). A clear synergistic effect was observed, as the experimental activity exceeded the value predicted by this model (Figure S5).

It is also worth noticing that phenylacetylene dimerization was favored when the catalyst was not active enough to fully promote the Sonogashira coupling. Although the bimetallic catalyst displayed similar conversion levels to the mechanical mixture, it exhibited distinct selectivity, showing a higher preference for product **1** (selectivity of 60% instead of 14% with the mechanical mixture) over product **2**. This behavior may be attributed to a Pd-Cu interaction within the bimetallic structure, absent in the physical mixture. This hypothesis is supported by XRD and HRTEM analyses (Figure 3, S4, S7), which revealed the formation of nanoscale bimetallic regions in the Pd-Cu catalyst, along with a pronounced decrease in copper particle size, compared to those of the 5%Cu/C–N^e material.

2.4 | Parametric Analysis

A parametric analysis of the mechanochemical-assisted Sonogashira process was performed by varying temperature, reaction time, screw rotation speed, and catalyst amount. All tests were carried out using the bimetallic 5%PdCu/C–N^e catalyst, selected for its superior performance in both conversion and selectivity toward product **1**.

2.4.1 | Temperature

Experiments were run under the conditions of Figure 8, except for the temperature which was set to vary from 80 to 115°C. Results are shown in Figure 9A,B. A pseudolinear increase in conversion from 8 to 98% was observed with increasing temperature in the explored range. Notably, at 80°C, the Sonogashira coupling was largely suppressed, and the dimerization of phenylacetylene became the dominant reaction. The increase of the temperature was also accompanied by the (expected) decrease of the selectivity toward product **1** due to the onset of the alkyne–alkyne coupling which originated product **2**. Based on these results, a temperature of 115°C was selected for the subsequent experiments. At this temperature, the conversion and selectivity toward product **1** were 98% and 60%, respectively.

2.4.2 | Residence Time

Residence time is critical in any continuous-flow process, as it directly affects catalyst-substrate contact, mixing efficiency, and, ultimately, reaction conversion and selectivity. Experiments were conducted under the conditions reported in Figure 8, varying the residence time from 30 to 60 min. Because the extruder reactor used in this work was 24 cm long, fine adjustment of the residence time without altering the applied mechanical torque (typically around 4 Nm) required operating under semi-continuous flow, in a loop configuration. In this setup, the material exiting the extruder was continuously recirculated to the feed zone, allowing extended processing times while maintaining steady mechanical and thermal conditions. Each experiment involved feeding a premixed batch of reactants and catalyst into the extruder, preheated to 115°C and operating at 100 rpm. The reaction time was measured from the moment of feeding, and the process was repeated until the desired residence time was reached.The results are reported in Figures 9C,D.

At the shortest explored reaction time (30 min), the Sonogashira reaction proceedeed with a selectivity toward product **1** above 95%. The conversion, however, was limited to 25% and the phenylacetylene dimerization occurred to a significant extent (48%). We hypothesized that the dimerization process was initially faster than the coupling because the former did not require the oxidative addition of the aryl halide, which is often considered the rate-determining step in the Sonogashira. As the reaction time increases, both the overall conversion and the product distribution improved significantly in favor of the cross-couplings (at 30, 45, and 60 min: conversions of 25%, 43%, and 98% and [**1** + **2**] amounts of 52, 60, and 90%, respectively). Prolonging

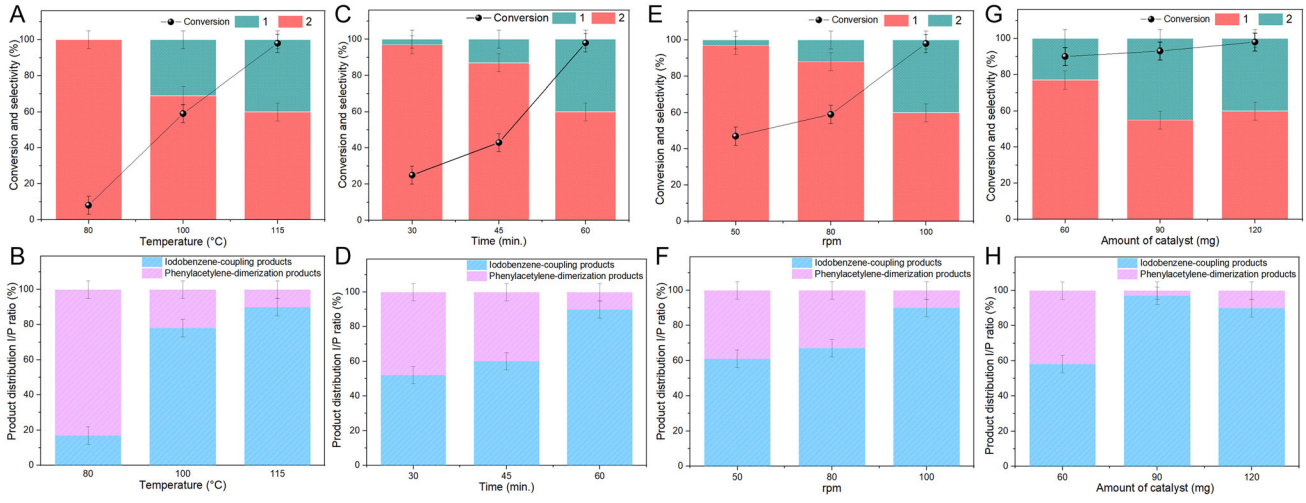

FIGURE 9 | Parametric analysis: temperature (A,B), time (C,D), rotation speed (E,F), and amount of catalyst (G,H) optimization study. Iodobenzene (5 mmol), phenylacetylene (1.5 eq.), K_2CO_3 (3 eq.), 5%PdCu/C–N^e. UP: representation of iodobenzene conversion and selectivity of cross-coupling products (1 and 2); DOWN: representation of product distribution I/P ratio, between iodobenzene-coupling products (**1** + **2**) and phenylacetylene dimerization product (**4**).

the reaction, however, brought about a progressive decrease of the selectivity toward the Sonogashira product **1** in favor of product **2**. A qualitative time-dependent analysis of this reaction, along with a comparison to the alkyne dimerization pathway, is reported in the Supporting Information (Figure S6).

2.4.3 | Screw Rotation Speed

Screw rotation speed (SRP), expressed in revolutions per minute (rpm) is a crucial parameter in mechanochemical extrusion processes since it directly affects the torque, which is a measure of the actual mechanochemical and the mechanical energy delivered to the reactants mixture. These aspects were confirmed also by our parametric analysis. Experiments were run under the conditions of Figure 8, by varying SPR from 50 to 100 rpm. Results are reported in Figures 9E,F. At the lowest explored rotation speed (50 rpm), a limited conversion (47%) was reached in line with a poor/insufficient supply of mechanical energy to the mixture. Under these conditions, compound **1** was substantially the sole observed cross-coupling product, but the competitive dimerization of phenylacetylene occurred to a large extent (39% of product distribution, see Figure 9F). Gradually increasing the screw speed to 100 rpm resulted in a quantitative reaction and, at the same time, significantly favored cross-coupling over dimerization, with product **2** becoming increasingly abundant compared to product **1**. These results were in line with the conversion/product distribution relationship already highlighted in Figure 8C,D.

Overall, the analysis indicated that the reaction was a thermal-mechanochemical-assisted process, where the combined effect of shear forces and temperature contributed to providing thermal and mechanical energy to improve reactant contact. The latter contact was further favored by the absence of solvent in the extruder. Moreover, the parametric studies show that product **2** originates from the secondary transformation of product **1**. As the reaction progresses and product **1** becomes increasingly available for further conversion, the amount of product **2** gradually rises, although product **1** remains the major component under the optimal conditions (selectivity of 60%). This sequential relationship explains why product **2** becomes more significant at higher overall conversions.

2.4.4 | The Catalyst Amount

The effect of catalyst loading was evaluated by designing experiments under the conditions of Figure 8, in which the amount of 5%PdCu/C–N^e was varied from 60 to 90 and 120 mg. This corresponded to a Pd/Iodobenzene molar ratio of 0.6, 0.7, and 1.1 mol%, respectively. The results are reported in Figures 9G,H. In the explored range, doubling the catalyst loading led to a very moderate increase in iodobenzene conversion, from 90 to 98%. However, the trend of the product distribution did not differ from that observed in Figures 8 and 9: at the lowest conversion (Pd/iodobenzene molar ratio = 0.6 mol%), the product distribution reflected the competition between the Sonogashira coupling and the dimerization of phenylacetylene, with products (**1** + **2**) and (**4**) obtained in relative amounts of 58% and 42%, respectively (Figure 9H). Among cross-coupling derivatives, compound **1** was the most abudant (77%). Under these conditions, it was possible that the relative low density of active sites hindered sequential reactions by reducing the probability for product **1** being further coordinated by Pd and converted to **2**. Increasing the catalyst amount suppressed the dimerization pathway in favor of the Sonogashira products (90 and 97% with Pd/Iodobenzene molar ratio of 0.7 and 1.1 mol% respectively) with compound **1** that was progressively transformed into compound **2**. At the highest catalyst loading tested (120 mg), the **1:2** relative ratio was ca 3:2.

These results highlighted the dual role of catalyst loading in mechanochemical extrusion reactions, where it modulated the balance between activity and selectivity by governing the extent of competing side reactions and promoting one cross-coupling process over another.

As these reactions were performed using a twin-screw extruder, essentially a continuous-flow mechanochemical reactor, productivity is also important to consider. Following multiparameter optimization, the highest productivity of product **1** from the Sonogashira reaction was achieved with 60 mg of catalyst, reaching 1.2 mol g_{Pd}^{-1} h^{-1} of product **1**. Nevertheless, considering that under these conditions a significant amount of dimerization products was also formed, a more comprehensive techno-economic assessment would be required. Under such an evaluation, the optimal compromise could be achieved using 90 mg of catalyst, which, although providing a lower productivity (0.6 mol g_{Pd}^{-1} h^{-1}), would facilitate the work-up, minimize the formation of dimerization by-products, and still use less catalyst than the 120 mg tested in this study. Under the latter conditions, a slightly lower productivity was observed (0.5 mol g_{Pd}^{-1} h^{-1}), as similar conversions were obtained despite the higher catalyst loading.

Overall, the parametric analysis of the investigated process led us to conclude that the most convenient conditions for cross-coupling were those indentified in Figure 8 (115°C, 1 h, 100 rpm, 120 mg of bimetallic catalyst), by which the dimerization of phenylacetilene was minimized and, at the same time, the cross-coupled products 1 and 2 were obtained in a 3:2 relative ratio

2.5 | The Comparison of Mechanochemical-Assisted Reaction to Batch Protocols under Conventional Heating

An additional study was carried out with the aim to compare the catalysts under the mechanochemical-assisted solvent-free Sonogashira conditions, with the same reaction under conventional batch conditions. Notably, the rheological properties of the reaction mixture did not allow a strict comparison among the two process modes, since solvent-free conditions could be achieved only by the mechanochemical treatment, and not by conventional heating. A batch procedure was therefore designed by adjusting a protocol from a study by Barros et al., in which different solvents were tested, with ethylene glycol identified as the most effective [78].

Batch experiments were carried out at the same T and t (115°C, 1 h) of mechanochemical reactions of Figure 8, using a mixture of iodobenzene (1 mmol), phenylacetylene (1.5 eq.), and ethylene glycol (10 mL) as the solvent [78]. Two model catalysts were used: i) the mechanical mixture of commercial 5%Pd/C with 5%Cu/C–N^e and ii) the bimetallic 5%PdCu/C–N^e sample, and the comparison was made with the commercial catalysts to provide a general reference and the bimetallic catalyst, which exhibited the best performance under mechanochemical setup.

In the conventional batch conditions, the catalyst obtained by the mechanical combination [5%Pd/C + 5%Cu/C–N^e] allowed to achieve an almost complete conversion (97%) with a 63% selectivity toward product **1**. This experiment also showed the formation of triphenylethylene (9%) derived from the hydroarylation of compound **1** with a second equivalent of iodobenzene. This transformation, previously described by Barros et al., typically required the presence of a reducing agent in the reaction medium, ethylene glycol in this case, and was not observed under reactive extrusion conditions.

In the presence of the bimetallic 5%PdCu/C–N^e catalyst, a comparatively lower conversion (40%) and a higher selectivity (97%) toward product **1** were reached.

These results highlighted that albeit commercial and 'chitin-derived' catalysts prepared in this work performed similarly under mechanochemical conditions, a different activity trend emerged from batch reactions.

The lower conversion observed with the 5%PdCu/C–N^e in batch was attributed to the more hydrophobic nature of the nitrogen-doped carbon support compared to the commercial carbon, which plausibly altered the suspension of the catalyst in polar protic ethylene glycol (compare Figure S7), thereby modifying the adsorption of reactants on the active sites. The moderate catalytic activity of 5%PdCu/C–N^e was also plausibly responsible for the almost exclusive formation of a single Sonogashira product **1**.

2.6 | Sustainability and Process Comparison

To ensure a fair assessment of the sustainability metrics, the extrusion protocol was compared directly with a batch reaction performed in ethylene glycol under identical thermal conditions (115°C, 1 h) and using the same 5%PdCu/C–N^e heterogeneous catalyst. This approach ensures that differences in E-factor (EF), space–time yield (STY), and specific energy consumption (SEC) originate from the intrinsic advantages of mechanochemical processing rather than from variations in catalyst formulation or operating temperature.

To evaluate the environmental impact and process efficiency of the two methods, the solvent-free mechanochemical protocol was benchmarked against the ethylene-glycol batch system. As summarized in Table 1, the extrusion process delivered a significantly higher net yield (59% vs. 39%), despite its lower selectivity (60% vs. 97%), owing to the near-quantitative conversion achieved under mechanochemical conditions (98%). From a sustainability standpoint, the EF of the extrusion protocol was calculated as 6.6, corresponding to a 26-fold reduction relative to the batch process (EF = 172). Notably, the batch EF was determined conservatively by excluding work-up solvents, meaning that the actual difference between the two approaches is likely even larger.

The mechanochemical method also exhibited superior process intensification, achieving a STY of 26.2 kg L^{-1} h^{-1}, ≈3.8 times higher than that of the batch system (6.9 kg L^{-1} h^{-1}). The SEC of the extrusion process was estimated using the nominal heating power of the ZE 12 HMI extruder (200 W), which represents a conservative upper bound for operation at 115°C (well below the 230°C nominal reference temperature). Under these assumptions, the extrusion route required almost 6 times less energy than the batch reaction conducted on a conventional heating plate (nominal 150 W), underscoring the enhanced energy efficiency of the continuous, solvent-free approach. Further details on the calculation of these metrics are provided in the Supporting Information.

2.7 | Substrate Scope

The substrate scope was evaluated using various aryl halides and terminal alkynes under the conditions of Figure 8 [115°C, 1 h, 100 rpm, aryl halide (5 mmol), alkyne (1.5 equivs.), and 3 eq. of K_2CO_3 (3 equivs.)], except for the catalyst (5%PdCu/C–N^e) the amount of which was set to 90 mg to minimize side reactions, particularly phenylacetylene dimerization. The results are reported in the Supporting Information (Table S2).

Low to very low conversions (in the range of 5–31%) were observed in the reactions involving 4-iodoanisole, 4-iodoacetophenone, and 4-chlorobenzene, while almost quantitative transformations (≥98%) of bromobenzene and bromotoluene were reached. These markedly fluctuating results were not clearly explained. However, a hypothesis was formulated based on the level of torque (approximately 4 Nm) required to ensure effective reactions in a twin-screw extruder, particularly the feed rate for C—X bond clevage in aryl halides, which is the rate-determining oxidative addition step. Torque is highly dependent on the rheological properties of the reaction mixture; thus, altering the total mass or composition of the mixture (e.g., by changing substrates) can significantly affect the reaction outcome. Morever, no conversion was observed with volatile alkynes such as propargyl alcohol or propargyl bromide because the low boiling point of these reactants limited effective interactions with the catalyst within the extrusion barrel.

These considerations led us to conclude that the investigated mechanochemical extrusion protocol was hardly generalizable

TABLE 1 | Sustainability comparison between Sonogashira reaction carried out under mechanochemical extrusion or under batch conditions.

Metric	Mechanochemical extrusion[a]	Batch process[b]	Improvement
Yield (%)	59[c]	39[d]	1.5x higher
STY (kg L^{-1} h^{-1})	26.2	6.9	3.8-fold increase
EF[e]	6.6	172	26-fold reduction
SEC (kWh kg^{-1})	381	2170	5.7-fold saving

[a]Iodobenzene (5 mmol), phenylacetylene (1.5 eq.), K_2CO_3 (3 eq.), 5%PdCu/C–N^e (120 mg), 115°C, 1 h, 100 rpm.
[b]Iodobenzene (1 mmol), phenylacetylene (1.5 eq.), K_2CO_3 (3 eq.), 5%PdCu/C–N^e (24 mg), 115°C, 1 h, 10 mL ethylene glycol.
[c]98% conversion, 60% selectivity.
[d]40% conversion, 97% selectivity.
[e]Calculated considering the reaction step only.

to diverse substrates and it rather required a case-by-case adjustement of the reaction conditions/parameters. Albeit with this limitation, the preliminary substrate scope analysis carried out in this work showed that the product distribution shifted toward phenylacetylene dimerization pathways when the applied torque was not sufficiently high to promote C—X bond cleavage (Table S2, entries 2, 3, and 6). However, when the overall conversion remained relatively low, the selectivity toward product **1** increased accordingly. For aryl bromides (Table S2, entries 4 and 5), higher torque values (5–6 Nm) led to nearly complete conversion; however, this excessive mechanical energy adversely affected selectivity, significantly increasing the formation of the aryl halide homocoupling product **3**. Under these conditions, the excess phenylacetylene also underwent partial cyclotrimerization, affording product **6** (Scheme S1). When different volatile alkynes were used (Table S2, entries 7 and 8), their rapid evaporation during processing allowed iodobenzene to undergo homocoupling, leading to substantial amounts of biphenyl (product **3**, Scheme S1).

2.8 | Catalyst Recycling

Catalysts recycling was carried out under the conditions of Figure 8, in the presence of the bimetallic 5%PdCu/C–N^e sample (90 mg), to minimize the extent of phenylacetylene dimerization and to operate just below full conversion (93%), while also aiming to use the minimal effective catalyst amount. Once a first reaction was complete, the mixture collected at the outlet of the extrusion barrel, was washed three times with diethyl ether and acetone. This allowed to recover both the catalyst and K_2CO_3 which were dried at 70°C for 12 h, and then reused for a second reaction.

From the first to the second test, a significant drop in the catalyst performance was observed, with the conversion of iodobenzene decreasing from 98% to 40% (Figure 10, recycle #1, box highlighted in yellow). Notably, the torque in the second run was low (approximately 1.0–1.5 Nm), indicating a reduced input of mechanical energy. This loss in performance was attributed to mechanical grinding of K_2CO_3 during the first reaction, which reduced the particle size of the base and altered the rheological properties and resistance of the mixture inside the extruder in the subsequent run.

To test this hypothesis, the reaction mixture from the second run was washed once with diethyl ether, three times with acetone, and then three times with water to remove any residual K_2CO_3. Fresh K_2CO_3 was added in the same amount (3 eq. compared to iodobenzene) used for the first reaction. Under these conditions, the torque increased to values comparable to the initial test (approximately 3.5–4.0 Nm), and both the conversion, cross-coupling selectivity, and product distribution were restored to initial values (cfr test 0 and recycle #2, Figure 10). For all subsequent recycling tests, fresh K_2CO_3 was used in each cycle, consistently maintaining catalyst's activity (recycles #3–6). Inductively Coupled Plasma-Optical Emission Spectroscopy (ICP-OES) analyses were performed on the fresh and spent catalysts, as well as on the post-reaction filtrates, to assess metal leaching and catalyst stability. The fresh material contained 4.8 wt% Pd and 4.6 wt% Cu, while the spent catalyst recovered after six consecutive runs showed 4.6 wt% Pd and 4.2 wt% Cu. ICP-OES of the filtered reaction mixtures showed Pd and Cu levels below the detection limit, confirming the absence of detectable leaching and supporting the observed recyclability of the catalyst.This behavior demonstrated the robustness and stability of the catalytic system under the conditions studied, without showing significant leaching or degradation effects, or loss of perfomance for at least five consecutive cycles.

2.9 | Phenyl Acetylene Dimerization

During the Sonogashira reaction under extrusion conditions, the formation of phenylacetylene dimers was consistently observed as a side reaction [85]. Although palladium-catalyzed alkyne dimerization is well established in solution-phase chemistry, it is generally limited by poor selectivity, harsh reaction conditions, and the need for special catalysts [72, 73]. In conventional solution-based protocols, the desired 1,3-diyne product is often accompanied by a range of byproducts, including various enynes, which can negatively affect the overall selectivity of the reaction [86–88]. Given the limited reports of this transformation under mechanochemical conditions, we carried out a dedicated investigation on the dimerization of phenylacetylene under solvent-free reactive extrusion conditions (Scheme 2). Observed products

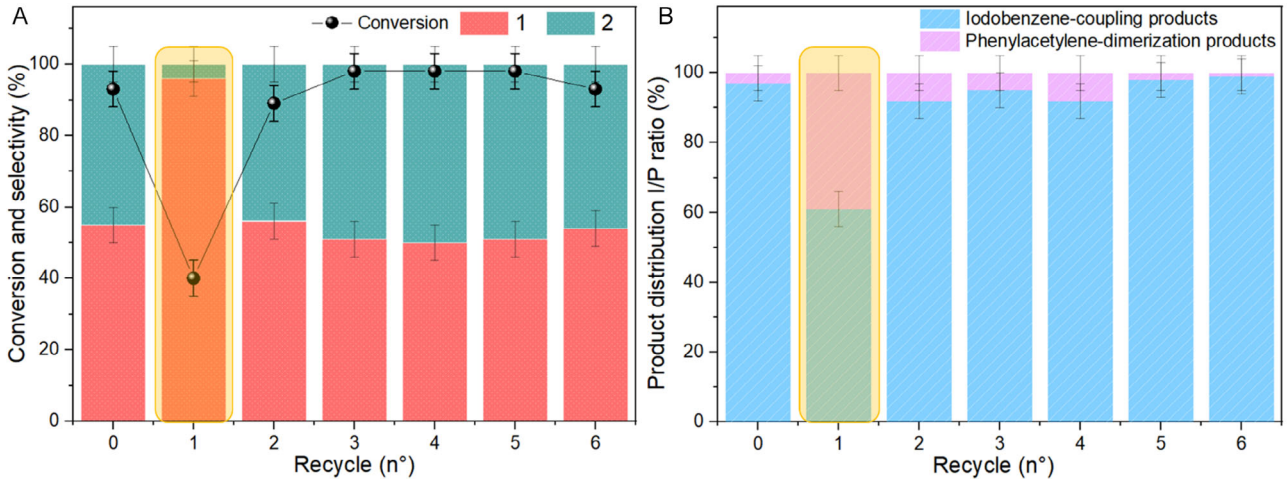

FIGURE 10 | Recyclability study of bimetallic catalyst. Iodobenzene (5 mmol), phenylacetylene (1.5 eq.), K_2CO_3 (3 eq.), 5%PdCu/C–N^e (90 mg), 115°C, 1 h, 100 rpm. Right: representation of iodobenzene conversion and selectivity of cross-coupling products (1 and 2). Left: representation of product distribution I/P ratio, between iodobenzene-coupling products (**1** + **2**) and dimerization-product (**4**).

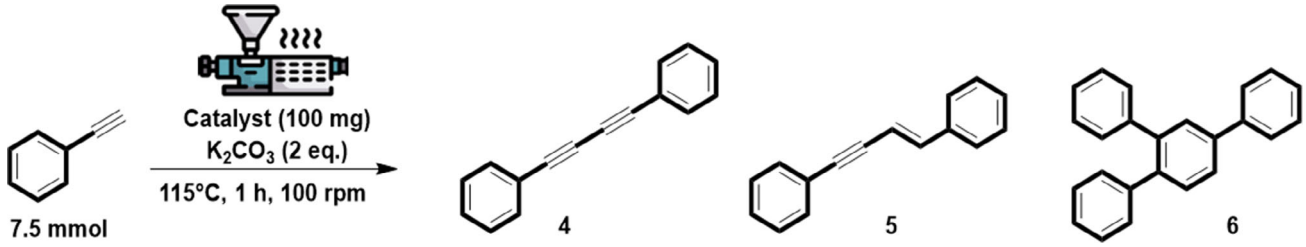

SCHEME 2 | Representative scheme of phenylacetylene dimerization or cyclotrimerization.

include the following: the oxidative homocoupling symmetrical 1,3-diyne **4**; a head-to-head dimerization product yielding a trans-enyne **5**; and a cyclotrimerization product (product **6**), which, to the best of our knowledge, has not been previously reported under mechanochemical conditions.

2.10 | Catalyst Screening

Initially, a catalyst screening was conducted using various synthesized materials under the same conditions as the Sonogashira coupling (100 rpm, 115°C, 1 h), using 7.5 mmol of phenylacetylene, 2.1 g of K_2CO_3 (2 eq.) and 100 mg of catalyst. As expected, the 5%Cu/C–N^e catalyst failed to achieve good conversion, likely proceeding through a Glaser-type mechanism [89, 90]. Interestingly, the screening revealed that the selectivity between the dimerization and cyclotrimerization pathways can be modulated by tuning the Pd loading (Figure 11). At 5 wt% Pd loading, the catalyst prepared via reactive extrusion and the one prepared by impregnation gave quantitative conversion and excellent selectivity toward product **6** (84 and 85%, respectively). In contrast, catalysts containing only 1 wt% Pd favored the formation of product **4**, with selectivity of 87 and 64%, and high conversions (80 and 83%), for the extruded and impregnated materials, respectively. Remarkably, the bimetallic 5%PdCu/C–N^e catalyst exhibited a synergistic effect between Pd and Cu, maximizing both the conversion and selectivity for product **4**, achieving a quantitative conversion and selectivity of 94%. In all tests, the formation of product **5** remained minimal (only exceeding 10% with the 5%Cu/C–N^e catalyst), indicating a clear preference for defined mechanochemical pathways under solvent-free reactive extrusion conditions.

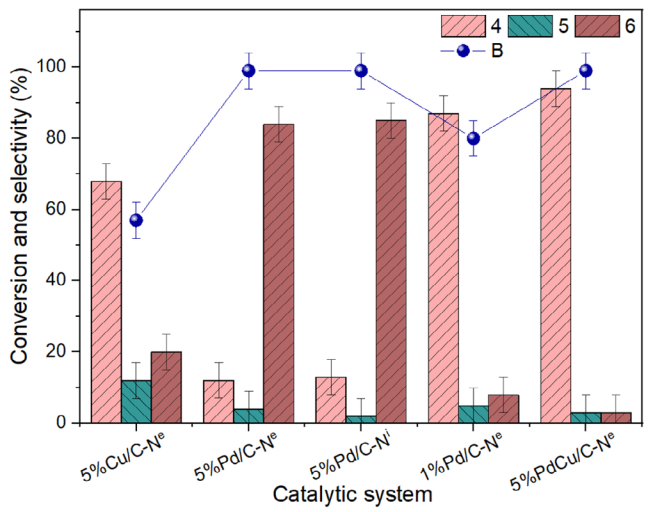

FIGURE 11 | Catalyst screening of phenylacetylene dimerization reaction. Phenylacetylene (7.5 mmol.), K_2CO_3 (2 eq.), catalyst (100 mg), 115°C, 1 h, 100 rpm.

2.11 | Parametric Analysis

Although the bimetallic catalyst displayed the best performance, the 1%Pd/C–N^e material was selected for further optimization (Figure 12) due to its higher sustainability, eliminating the need for copper and reducing palladium usage fivefold. Despite not reaching full conversion, this catalyst delivered a productivity of 5.2 mol g_{Pd}^{-1} h^{-1} for product **4**, outperforming the bimetallic system (1.4 mol g_{Pd}^{-1} h^{-1}). The effect of the rpm was first evaluated at 115°C for 1 h. Increasing rpm from 100 to 150 raised the torque from an average of 3–4 Nm, without significantly affecting conversion, but it did markedly alter the selectivity, resulting in a product distribution of 31, 16, and 53% for products **4**, **5**, and **6**, respectively.

The influence of temperature at 100 rpm was then investigated at 80°C, 100°C, and 115°C. At 80°C, the conversion remained low (44%), accompanied by a drop in selectivity (51 and 31% for products **4** and **5**, respectively), and also with the appearance of product **6** (18%). This behavior was attributed to the higher torque at lower temperatures, which enabled cyclotrimerization but limited the overall conversion. Conversely, at 115°C the reduced viscosity of the mixture lowered the torque and the mechanochemical input, but the higher temperature allowed reaching 80% conversion and 87% selectivity toward product **4**. The optimal conditions were found at 100°C, where the balance between torque and temperature afforded the highest conversion (83%) and excellent selectivity (96%) toward product **4**, with the formation of product **6**.

Finally, the residence time in the extruder was studied. As already observed for the Sonogashira coupling, the phenylacetylene dimerization showed a short induction period: after 30 min, the conversion reached 67% with nearly complete selectivity toward product **4** (99%). At 60 and 90 min, conversions increased to 83 and 87%, while the selectivity remained high (96% for product **4** in both cases).

Overall, 100 rpm, 100°C and 60 min proved to be the optimal conditions, combining high conversion with excellent selectivity toward product **4**, while avoiding the formation of undesired byproducts. Under these optimized conditions, a remarkably high productivity of 6 mol g_{Pd}^{-1} h^{-1} was achieved for product **4**.

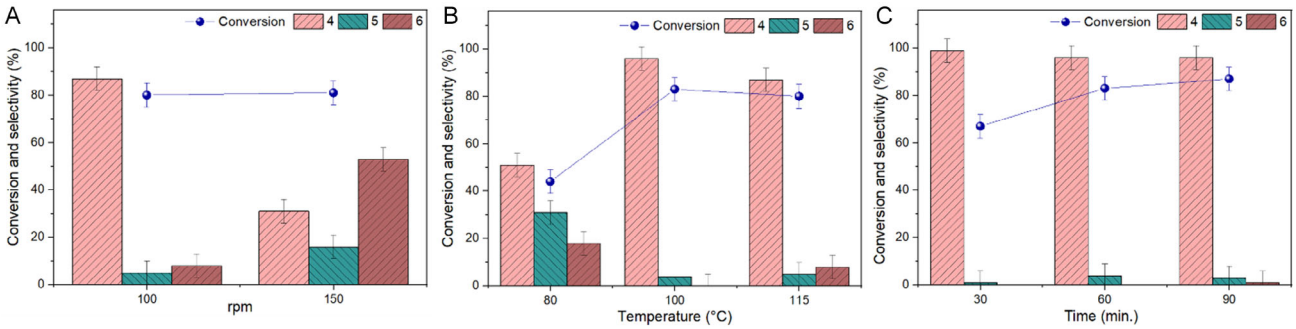

FIGURE 12 | Influence of rpm, temperature, and time in dimerization reaction of phenylacetylene. Phenylacetylene (7.5 mmol.), K_2CO_3 (2 eq.), 1%Pd/C–N^e (100 mg).

3 | Experimental

3.1 | Synthesis of Materials

Palladium (Pd), copper (Cu), and bimetallic Pd-Cu nanoparticles supported on nitrogen-doped carbon (C–N) were synthesized using different precursor loadings to achieve 1 and 5 wt% metal contents. To obtain these loadings, 0.1 mmol and 0.5 mmol of palladium(II) acetate ($Pd(OAc)_2$) were used, respectively. Following a protocol previously reported by our group, three distinct preparation methods were applied: impregnation, solution-based synthesis, and mechanochemical extrusion [17].

3.1.1 | Impregnation Method (Pd/C–N^i)

The desired amount of metal precursor was dissolved in 15 mL of 2-propanol, and 5 g of chitin were added. The mixture was aged overnight at room temperature, followed by drying in a vacuum oven at 100°C. The resulting solid was thermally treated at 500°C for 1 h under N_2 flow (10 mL/min) with a heating rate of 5°C/min.

3.1.2 | Solution Method (Pd/C–N^s)

The metal precursor was dissolved in 60 mL of 2-propanol along with 1 g of EDTA. Then, 5 g of chitin were added, and the mixture was refluxed under stirring at 80°C for 9 h. The suspension was filtered, and the solid was dried overnight at 100°C and subsequently heated at 500°C for 1 h under N_2 flow.

3.1.3 | Mechanochemical Extrusion Method (Pd/C–N^e)

This procedure involved mixing 5 g of chitin with the metal precursor and 15 mL of ethylene glycol, followed by processing in a ZE 12 HMI corotating twin-screw extruder (Three Tec, Seon, Switzerland) at 200°C and 50 rpm. The extrudate was further heated at 500°C for 1 h under N_2 flow, using a heating rate of 5°C/min.

3.2 | Characterization Techniques

XRD patterns were recorded on a Bruker AXS D8 Advance diffractometer using Cu Kα radiation and a LynxEye detector. Scans were carried out from $2\theta = 8°$ to 80° with a step size of 0.08°/min to investigate the crystalline structure.

XPS measurements were performed using a VersaProbe II (Physical Electronics) equipped with an Al Kα source (under a vacuum of 10^{-7} Pa). Binding energies were calibrated against the C 1*s* peak at 284.8 eV. High-resolution spectra were collected using a hemispherical analyzer at a constant pass energy of 29.35 eV over a 200 µm analysis area. Data were processed using the PHI ACCESS ESCA-F V6 software with Shirley background subtraction and peak fitting using mixed Gaussian–Lorentzian profiles. The Pd content in the catalysts was quantified using a PerkinElmer Avio 550 Max ICP-OES system.

The textural properties of the samples were analyzed at −196°C using a Micromeritics ASAP 2000 instrument. Samples were degassed at 120°C for 2 h prior to measurement. The specific surface areas were calculated using the BET method, the pore volumes were determined from the adsorption isotherms, and the pore size distributions were estimated using the Barrett, Joyner, and Halenda (BJH) algorithm available in the integrated Micromeritics software.

High-resolution transmission electron microscopy (HRTEM) and scanning transmission electron microscopy (STEM) images were acquired with a TALOS F200x microscope, both operating at 200 kV and 200 nA. The mapping images were obtained by EDX Super-X system with 4 X-ry detectors and a X-FEG beam. The particle size distribution was obtained from EDX images by the Image J software, counting between 500 and 1000 particles selected in several different parts of each sample.

3.3 | Reaction Procedure

Mechanochemical reactions were carried out using a ZE 12 HMI corotating twin-screw extruder (ThreeTec, Seon, Switzerland). The instrument was equipped with a modular screw configuration (diameter 12 mm, L/D = 20), consisting of conveying elements and two kneading blocks staggered at 60° and 90°, respectively. The screw speed was set to 100 rpm unless otherwise specified. During operation, the extruder torque typically ranged between 1 and 6 Nm, depending on the formulation, viscosity, and catalyst loading; under optimized Sonogashira conditions, torque values stabilized around 3.5–4.0 Nm. The residence time under optimized conditions was controlled by loop recirculation. Temperature along the barrel was monitored by embedded thermocouples and maintained at 115°C (±1°C) using four independent heating zones, ensuring uniform thermal input along the barrel during the mechanochemical process.

The reaction mixture was prepared by combining K_2CO_3 (3 eq., 2.1 g), 100 mg of Pd/C–N^e, 120 mg of Cu/C–N^e, 548 µL of

iodobenzene, and 778 μL of phenylacetylene in a beaker. This mixture was then introduced into the twin-screw extruder. The extruder was operated at 115°C and 100 rpm for 1 h initially. In subsequent experiments, parameters such as rpm, reaction time, and temperature were varied to study their effect on conversion. The extrudate was recovered using or diethyl ether. The dimerization reaction was carried out using the same procedure, with the only difference being the exclusion of iodobenzene from the reaction mixture.

Both qualitative and quantitative analyses were performed. Conversion and selectivity were determined by GC-FID (analyses were conducted with an Elite-624 capillary column ($L = 30$ m, Ø = 0.32 mm, film thickness = 1.8 μm), and product structures were confirmed by GC–MS, (performed with an HP5-MS capillary column ($L = 30$ m, Ø = 0.32 mm, film thickness = 0.25 μm) using EI (70 eV)).

^{1}H and ^{13}C NMR spectra were recorded on a Bruker Advance III HD 400 WB spectrometer equipped with a 4 mm CP/MAS probe, operating at 400 MHz and 101 MHz, respectively.

4 | Conclusions

Mechanochemical extrusion is a powerful and sustainable platform for the preparation of mono- and bimetallic Pd/Cu catalysts supported on nitrogen-doped carbons. Solvent-free extrusion enables the formation of uniformly dispersed nanoparticles with strong metal–support and metal–metal interactions, while producing smaller particle sizes and larger surface areas compared to conventional solution-based methods. Under continuous mechanochemical flow, the bimetallic Pd-Cu catalyst exhibited superior activity and selectivity in the Sonogashira coupling of iodobenzene with phenylacetylene compared to a physical mixture of the monometallic Pd and Cu catalysts, demonstrating a clear synergistic effect arising from the direct contact and intimate metal–metal interactions within the bimetallic material. A detailed parametric study revealed that mechanical energy plays a pivotal role in determining reaction outcomes and product distribution. Mechanochemical extrusion enables transformations that are difficult to achieve under conventional batch conditions, including the controlled formation of product **2**, which is challenging to obtain under mild solution-phase protocols.

Looking forward, the mechanochemical extrusion approach offers significant potential for scale-up and industrial applications, where longer extruder configurations could further enhance residence time, mass transfer, and reaction efficiency. The tunability of catalyst composition and distribution also opens us opportunities to design tailored bimetallic or multimetallic systems for other challenging cross-coupling and C–H functionalization reactions. Moreover, the solvent-free and energy-efficient nature of extrusion aligns with the green chemistry principles, making it a promising strategy for sustainable heterogeneous catalysis. Future studies could explore the integration of in-line monitoring techniques to further optimize reaction conditions and provide real-time insights into mechanistic pathways, ultimately advancing the development of continuous-flow mechanochemical processes for a wide range of synthetic transformations.

Acknowledgments

D.R.-P. received funding from the European Union's Horizon2020 Research and Innovation Programme under the Marie Sklodowska-Curie Cofund Grant Agreement No. 945361. O.T. acknowledges the National Doctoral Program in Design for Made in Italy: Identity, Innovation and Sustainability for financial support. D.B.-P. and E.R.-C. thank to the Spanish Ministry of Science and Innovation, project PID2021-126235OB–C32 funded by MCIN/AEI/10.13039/501100011033 and FEDER funds.

Conflicts of Interest

The authors declare no conflicts of interest.

Data Availability Statement

The data that support the findings of this study are available from the corresponding author upon reasonable request.

References

1. M. Farhang, A. R. Akbarzadeh, M. Rabbani, and A. M. Ghadiri, "A Retrospective-Prospective Review of Suzuki–Miyaura Reaction: From Cross-Coupling Reaction to Pharmaceutical Industry Applications," *Polyhedron* 227 (2022): 116124.

2. M. Ashraf, M. S. Ahmad, Y. Inomata, N. Ullah, M. N. Tahir, and T. Kida, "Transition Metal Nanoparticles as Nanocatalysts for Suzuki, Heck and Sonogashira Cross-Coupling Reactions," *Coordination Chemistry Reviews* 476 (2023): 214928.

3. I. Ghosh, N. Shlapakov, T. A. Karl, et al., "General Cross-Coupling Reactions with Adaptive Dynamic Homogeneous Catalysis," *Nature* 619 (2023): 87–93.

4. L. E. Zetzsche, J. A. Yazarians, S. Chakrabarty, et al., "Biocatalytic Oxidative Cross-Coupling Reactions for Biaryl Bond Formation," *Nature* 603 (2022): 79–85.

5. C. Kieffer, P. Verhaeghe, N. Primas, et al., "Sonogashira Cross-Coupling Reaction in 4-Chloro-2-Trichloromethylquinazoline Series is Possible despite a Side Dimerization Reaction," *Tetrahedron* 69 (2013): 2987–2995.

6. F. Yan, X. Zhang, D. Li, N. Zhu, and H. Bao, "Recent Applications of the Sonogashira Reaction in the Synthesis of Drugs and Their Derivatives: A Review," *Applied Organometallic Chemistry* 39 (2025): e7932.

7. P. Devendar, R. Y. Qu, W. M. Kang, B. He, and G. F. Yang, "Palladium-Catalyzed Cross-Coupling Reactions: A Powerful Tool for the Synthesis of Agrochemicals," *Journal of Agricultural and Food Chemistry* 66 (2018): 8914–8934.

8. Q. Yang, Y. Zhao, and D. Ma, "Cu-Mediated Ullmann-Type Cross-Coupling and Industrial Applications in Route Design, Process Development, and Scale-up of Pharmaceutical and Agrochemical Processes," *Organic Process Research & Development* 26 (2022): 1690–1750.

9. S. Vásquez-Céspedes, R. C. Betori, M. A. Cismesia, J. K. Kirsch, and Q. Yang, "Heterogeneous Catalysis for Cross-Coupling Reactions: An Underutilized Powerful and Sustainable Tool in the Fine Chemical Industry," *Organic Process Research & Development* 25 (2021): 740–753.

10. K. Islam, B. K. Bhunia, G. Mandal, et al., "Room-Temperature, Copper-Free, and Amine-Free Sonogashira Reaction in a Green Solvent: Synthesis of Tetraalkynylated Anthracenes and In Vitro Assessment of Their Cytotoxic Potentials," *ACS Omega* 8 (2023): 16907–16926.

11. C. A. Fleckenstein and H. Plenio, "Aqueous/Organic Cross Coupling: Sustainable Protocol for Sonogashira Reactions of Heterocycles," *Green Chemistry* 10 (2008): 563.

12. P. Adler, T. Dumas, P.-A. Deyris, et al., "II- from Ecological Recycling of Pd to Greener Sonogashira Cross-Coupling Reactions," *Journal of Cleaner Production* 293 (2021): 126164.

13. G. Strappaveccia, L. Luciani, E. Bartollini, A. Marrocchi, F. Pizzo, and L. Vaccaro, "γ-Valerolactone as an Alternative Biomass-Derived Medium for the Sonogashira Reaction," *Green Chemistry* 17 (2015): 1071–1076.

14. A. Dewan, M. Sarmah, U. Bora, and A. J. Thakur, "A Green Protocol for Ligand, Copper and Base Free Sonogashira Cross-Coupling Reaction," *Tetrahedron Letters* 57 (2016): 3760–3763.

15. R. R. A. Bolt, J. A. Leitch, A. C. Jones, W. I. Nicholson, and D. L. Browne, "Continuous Flow Mechanochemistry: Reactive Extrusion as an Enabling Technology in Organic Synthesis," *Chemical Society Reviews* 51 (2022): 4243–4260.

16. T. Seo, K. Kubota, and H. Ito, "Mechanochemistry-Directed Ligand Design: Development of a High-Performance Phosphine Ligand for Palladium-Catalyzed Mechanochemical Organoboron Cross-Coupling," *Journal of the American Chemical Society* 145 (2023): 6823–6837.

17. O. Trentin, D. Ballesteros-Plata, E. Rodríguez-Castellón, et al., "Upcycling of Chitin to Cross-Coupling Catalysts: Tailored Supports and Opportunities in Mechanochemistry," *ChemSusChem* 18 (2025): e202401255, https://doi.org/10.1002/cssc.202401255.

18. O. Trentin, D. Polidoro, A. Perosa, E. Rodríguez-Castellon, D. Rodríguez-Padrón, and M. Selva, "Mechanochemistry through Extrusion: Opportunities for Nanomaterials Design and Catalysis in the Continuous Mode," *Chemistry* 5 (2023): 1760–1769.

19. C. Espro and D. Rodríguez-Padrón, "Re-Thinking Organic Synthesis: Mechanochemistry as a Greener Approach," *Current Opinion in Green and Sustainable Chemistry* 30 (2021): 100478.

20. Y. Gao, C. Feng, T. Seo, K. Kubota, and H. Ito, "Efficient Access to Materials-Oriented Aromatic Alkynes via the Mechanochemical Sonogashira Coupling of Solid Aryl Halides with Large Polycyclic Conjugated Systems," *Chemical Science* 13 (2022): 430–438.

21. W. Pickhardt, E. Siegfried, S. Fabig, et al., "The Sonogashira Coupling on Palladium Milling Balls—A New Reaction Pathway in Mechanochemistry," *Angewandte Chemie International Edition* 62 (2023): e202301490.

22. X. Zhang, Q. Liu, J. Gao, et al., "Electromagnetic Mill Promoted Mechanochemical Sonogashira Coupling Reaction and Mechanism Insight into the Catalytic Complex," *Advanced Synthesis & Catalysis* 367 (2025): e202500100.

23. R. H. Hastings, M. M. Mokhtar, A. Ruggles, et al., "Investigation of Mechanochemical Sonogashira Couplings—From Batch Solution to Continuous Reactive Extrusion through Ball-Milling Optimization," *Organic Process Research & Development* 27 (2023): 1667–1676.

24. A. Rubin Pedrazzo, F. Trotta, G. Hoti, F. Cesano, and M. Zanetti, "Sustainable Mechanochemical Synthesis of β-Cyclodextrin Polymers by Twin Screw Extrusion," *Environmental Science and Pollution Research* 29 (2022): 251–263.

25. D. Daurio, C. S. Jacobsen, K. Nagapudi, et al., "Application of Mechanochemistry to Green, Scalable, and Continuous Manufacturing of Pharmaceutically Relevant Peptides by Twin-Screw Extrusion," *Journal of Pharmaceutical Sciences* 114 (2025): 103941.

26. Y. Zhuang, N. Saadatkhah, M. S. Morgani, et al., "Experimental Methods in Chemical Engineering: Reactive Extrusion," *Canadian Journal of Chemical Engineering* 101 (2023): 59–77.

27. C. Martin, Twin Screw Extrusion for Pharmaceutical Processes, 2013, 47–79.

28. D. E. Crawford, C. K. G. Miskimmin, A. B. Albadarin, G. Walker, and S. L. James, "Organic Synthesis by Twin Screw Extrusion (TSE): Continuous, Scalable and Solvent-Free," *Green Chemistry* 19 (2017): 1507–1518.

29. K. S. Guiao, A. Gupta, C. Tzoganakis, and T. H. Mekonnen, "Reactive Extrusion as a Sustainable Alternative for the Processing and Valorization of Biomass Components," *Journal of Cleaner Production* 355 (2022): 131840.

30. T. Vialon, H. Sun, G. J. M. Formon, et al., "Upcycling Polyolefin Blends into High-Performance Materials by Exploiting Azidotriazine Chemistry Using Reactive Extrusion," *Journal of the American Chemical Society* 146 (2024): 2673–2684.

31. E. C. Gaudino, G. Grillo, M. Manzoli, S. Tabasso, S. Maccagnan, and G. Cravotto, "Mechanochemical Applications of Reactive Extrusion from Organic Synthesis to Catalytic and Active Materials," *Molecules* 27-27 (2022): 449.

32. F. Zorzetto, D. Ballesteros-Plata, A. Perosa, E. Rodríguez-Castellón, M. Selva, and D. Rodríguez-Padrón, "Orthogonal Assisted Tandem Reactions for the Upgrading of Bio-Based Aromatic Alcohols Using Chitin Derived Mono and Bimetallic Catalysts," *Green Chemistry* 26 (2024): 5221–5238.

33. L. Chen, M. Regan, and J. Mack, "The Choice is Yours: Using Liquid-Assisted Grinding To Choose between Products in the Palladium-Catalyzed Dimerization of Terminal Alkynes," *ACS Catalysis* 6 (2016): 868–872.

34. D. Polidoro, D. Rodriguez-Padron, A. Perosa, R. Luque, and M. Selva, "Chitin-Derived Nanocatalysts for Reductive Amination Reactions," *Materials* 16 (2023): 575, https://doi.org/10.3390/ma16020575.

35. J. Lv, X. Lv, M. Ma, D.-H. Oh, Z. Jiang, and X. Fu, "Chitin and Chitin-Based Biomaterials: A Review of Advances in Processing and Food Applications," *Carbohydrate Polymers* 299 (2023): 120142.

36. T. Jin, M. Hicks, D. Kurdyla, S. Hrapovic, E. Lam, and A. Moores, "Palladium Nanoparticles Supported on Chitin-Based Nanomaterials as Heterogeneous Catalysts for the Heck Coupling Reaction," *Beilstein Journal of Organic Chemistry* 16 (2020): 2477–2483.

37. D. Polidoro, D. Ballesteros-Plata, A. Perosa, E. Rodríguez-Castellón, D. Rodríguez-Padrón, and M. Selva, "Controlled Alcohol Oxidation Reactions by Supported Non-Noble Metal Nanoparticles on Chitin-Derived N-Doped Carbons," *Catalysis Science & Technology* 13 (2023): 2223–2238.

38. Q. Wu, L. Wang, B. Zhao, L. Huang, S. Yu, and A. J. Ragauskas, "Highly Selective Hydrogenation of Phenol to Cyclohexanone over a Pd-Loaded N-Doped Carbon Catalyst Derived from Chitosan," *Journal of Colloid and Interface Science* 605 (2022): 82–90.

39. Z. Tan, R. Wang, S. Yang, Z. Shi, and D. Wang, "Fabrication of Cu-Cu_2ON Doped Carbon with High Photo-Fenton Catalytic Activity Using a Cu-Nicotinic Acid Framework: Insight into Structural Transformation," *Journal of Molecular Structure* 1337 (2025): 142248.

40. J. Kim, S. Noh, and J. H. Shim, "Nitrogen-Doped Carbon Dot/Activated Carbon Nanotube-Supported Copper Nanoparticles as an Efficient Electrocatalyst for the Oxygen Reduction Reaction," *Journal of Electroanalytical Chemistry* 937 (2023): 117423.

41. X. Zhang, K. Li, P. Yan, Z. Liu, and L. Pu, "N-Type Cu_2O Doped Activated Carbon as Catalyst for Improving Power Generation of Air Cathode Microbial Fuel Cells," *Bioresource Technology* 187 (2015): 299–304.

42. D. A. Bulushev, A. L. Chuvilin, V. I. Sobolev, et al., "Copper on Carbon Materials: Stabilization by Nitrogen Doping," *Journal of Materials Chemistry A* 5 (2017): 10574–10583.

43. Z. Bai, L. Niu, Q. Zhang, et al., "Hollow PdCu Nanocubes Supported by N-Doped Graphene: A Surface Science and Electrochemical Study," *International Journal of Hydrogen Energy* 40 (2015): 14305–14313.

44. Q. Zhao, L. Liu, R. Liu, and L. Zhu, "PdCu Nanoalloy Immobilized in ZIF-Derived N-Doped Carbon/Graphene Nanosheets: Alloying Effect on Catalysis," *Chemical Engineering Journal* 353 (2018): 311–318.

45. V. G. Baldovino-Medrano, V. Niño-Celis, and R. Isaacs Giraldo, "Systematic Analysis of the Nitrogen Adsorption–Desorption Isotherms Recorded for a Series of Materials Based on Microporous–Mesoporous

Amorphous Aluminosilicates Using Classical Methods," *Journal of Chemical and Engineering Data* 68 (2023): 2512–2528.

46. R. Bardestani, G. S. Patience, and S. Kaliaguine, "Experimental Methods in Chemical Engineering: Specific Surface Area and Pore Size Distribution Measurements—BET, BJH, and DFT," *Canadian Journal of Chemical Engineering* 97 (2019): 2781–2791.

47. D. Polidoro, A. Perosa, E. Rodríguez-Castellón, et al., "Metal-Free *N*-Doped Carbons for Solvent-Less CO_2 Fixation Reactions: A Shrimp Shell Valorization Opportunity," *ACS Sustainable Chemistry & Engineering* 10 (2022): 13835–13848.

48. R. Kumar, J. H. Oh, H. J. Kim, et al., "Nanohole-Structured and Palladium-Embedded 3D Porous Graphene for Ultrahigh Hydrogen Storage and CO Oxidation Multifunctionalities," *ACS Nano* 9 (2015): 7343–7351.

49. X. Gao, Z. Shen, G. Chang, Z. Li, and H. Zhao, "Mechanochemistry Induced Pore Regulation and Pyridinic Nitrogen Doping in Anthracite Derived Carbon for Sodium Storage," *Diamond and Related Materials* 130 (2022): 109481.

50. S. Dong, X. Gu, Y. Li, et al., "Mechanically Induced Surface Defect Engineering in Expanded Graphite to Boost the Low-Voltage Intercalation Kinetics for Advanced Potassium-Ion Batteries," *Carbon* 232 (2025): 119791.

51. H. Chen, Q. Cao, Z. Ye, et al., "Making 2-D Materials Mechanochemically by Twin-Screw Extrusion: Continuous Exfoliation of Graphite to Multi-Layered Graphene," *Advanced Materials Technologies* 9 (2024): 2301780.

52. C. Schneidermann, N. Jäckel, S. Oswald, L. Giebeler, V. Presser, and L. Borchardt, "Solvent-Free Mechanochemical Synthesis of Nitrogen-Doped Nanoporous Carbon for Electrochemical Energy Storage," *ChemSusChem* 10 (2017): 2416–2424.

53. Z. He, B. Dong, W. Wang, et al., "Elucidating Interaction between Palladium and N-Doped Carbon Nanotubes: Effect of Electronic Property on Activity for Nitrobenzene Hydrogenation," *ACS Catalysis* 9 (2019): 2893–2901.

54. S. Mao, C. Wang, and Y. Wang, "The Chemical Nature of N Doping on N Doped Carbon Supported Noble Metal Catalysts," *Journal of Catalysis* 375 (2019): 456–465.

55. R. Arrigo, M. E. Schuster, Z. Xie, et al., "Nature of the N–Pd Interaction in Nitrogen-Doped Carbon Nanotube Catalysts," *ACS Catalysis* 5 (2015): 2740–2753.

56. Y. Shi, Y.-F. Hu, J. Ye, et al., "Stabilization of Pd^0 by Cu Alloying: Theory-Guided Design of Pd_3Cu Electrocatalyst for Anodic Methanol Carbonylation," *Angewandte Chemie* 136 (2024): e202401311.

57. X. Xiao, J. Gao, S. Xi, et al., "Experimental and In Situ DRIFTs Studies on Confined Metallic Copper Stabilized Pd Species for Enhanced CO_2 Reduction to Formate," *Applied Catalysis B: Environmental* 309 (2022): 121239.

58. M. Fernández-García, J. A. Anderson, and G. L. Haller, "Alloy Formation and Stability in Pd−Cu Bimetallic Catalysts," *Journal of Physical Chemistry* 100 (1996): 16247–16254.

59. R. Shi, J. Zhao, S. Liu, et al., "Nitrogen-Doped Graphene Supported Copper Catalysts for Methanol Oxidative Carbonylation: Enhancement of Catalytic Activity and Stability by Nitrogen Species," *Carbon* 130 (2018): 185–195.

60. N. E. Şahin, C. Comminges, S. Arrii, T. W. Napporn, and K. B. Kokoh, "CO_2-to-HCOOH Electrochemical Conversion on Nanostructured Cu_xPd_{100-x}/Carbon Catalysts," *ChemElectroChem* 8 (2021): 1362–1368.

61. C. Goswami, H. Saikia, B. Jyoti Borah, et al., "Boosting the Electrocatalytic Activity of Pd/C by Cu Alloying: Insight on Pd/Cu Composition and Reaction Pathway," *Journal of Colloid and Interface Science* 587 (2021): 446–456.

62. T. J. Colacot, "The 2010 Nobel Prize in Chemistry: Palladium-Catalysed Cross-Coupling," *Platinum Metals Review* 55 (2011): 84–90.

63. R. F. Heck, "Palladium-Catalyzed Reactions of Organic Halides with Olefins," *Accounts of Chemical Research* 12 (1979): 146–151.

64. I. S. Patel, G. Ganesan, and S. Jain, "Catalytic Advancements: Optimizing Pd-Based Cross-Coupling Reactions Through Flow Chemistry," *Organic Process Research & Development* 28 (2024): 3464–3508.

65. A. Srivastava, H. Kaur, H. Pahuja, T. M. Rangarajan, R. S. Varma, and S. Pasricha, "Optimal Exploitation of Supported Heterogenized Pd Nanoparticles for C-C Cross-Coupling Reactions," *Coordination Chemistry Reviews* 507 (2024): 215763.

66. C. S. Horbaczewskyj and I. J. S. Fairlamb, "Pd-Catalyzed Cross-Couplings: On the Importance of the Catalyst Quantity Descriptors, mol% and ppm," *Organic Process Research & Development* 26 (2022): 2240–2269.

67. Q. D. Wang, S. X. Zhang, Z. W. Zhang, et al., "Palladium-Catalyzed Sonogashira Coupling of a Heterocyclic Phosphonium Salt with a Terminal Alkyne," *Organic Letters* 24 (2022): 4919–4924.

68. D. Faust Akl, D. Poier, S. C. D'Angelo, et al., "Assessing the Environmental Benefit of Palladium-Based Single-Atom Heterogeneous Catalysts for Sonogashira Coupling," *Green Chemistry* 24 (2022): 6879–6888.

69. D. Poier, D. F. Akl, E. Lucas, et al., "Reaction Environment Design for Multigram Synthesis via Sonogashira Coupling over Heterogeneous Palladium Single-Atom Catalysts," *ACS Sustainable Chemistry & Engineering* 11 (2023): 16935–16945.

70. P. Y. Choy, K. B. Gan, and F. Y. Kwong, "Recent Expedition in Pd-Catalyzed Sonogashira Coupling and Related Processes†," *Chinese Journal of Chemistry* 41 (2023): 1099–1118.

71. F. Alonso and M. Yus, "Heterogeneous Catalytic Homocoupling of Terminal Alkynes," *ACS Catalysis* 2 (2012): 1441–1451.

72. H. A. Stefani, A. S. Guarezemini, and R. Cella, "Homocoupling Reactions of Alkynes, Alkenes and Alkyl Compounds," *Tetrahedron* 66 (2010): 7871–7918.

73. J.-H. Li, Y. Liang, and Y.-X. Xie, "Efficient Palladium-Catalyzed Homocoupling Reaction and Sonogashira Cross-Coupling Reaction of Terminal Alkynes under Aerobic Conditions," *Journal of Organic Chemistry* 70 (2005): 4393–4396.

74. L. Wang, Y. Zhang, L. Liu, and Y. Wang, "Palladium-Catalyzed Homocoupling and Cross-Coupling Reactions of Aryl Halides in Poly(ethylene Glycol)," *Journal of Organic Chemistry* 71 (2006): 1284–1287.

75. N. W. J. Scott, M. J. Ford, N. Jeddi, et al., "A Dichotomy in Cross-Coupling Site Selectivity in a Dihalogenated Heteroarene: Influence of Mononuclear Pd, Pd Clusters, and Pd Nanoparticles—the Case for Exploiting Pd Catalyst Speciation," *Journal of the American Chemical Society* 143 (2021): 9682–9693.

76. K. Kirchner, M. J. Calhorda, R. Schmid, and L. F. Veiros, "Mechanism for the Cyclotrimerization of Alkynes and Related Reactions Catalyzed by CpRuCl," *Journal of the American Chemical Society* 125 (2003): 11721–11729.

77. J. S. Doll, R. Eichelmann, L. E. Hertwig, et al., "Iron-Catalyzed Trimerization of Terminal Alkynes Enabled by Pyrimidinediimine Ligands: A Regioselective Method for the Synthesis of 1,3,5-Substituted Arenes," *ACS Catalysis* 11 (2021): 5593–5600.

78. J. C. Barros, A. L. F. de Souza, P. G. de Lima, J. F. M. da Silva, and O. A. C. Antunes, "Selectivity Studies in the Reaction between Iodobenzene and Phenylacetylene: Sonogashira Coupling Vs Hydroarylation," *Applied Organometallic Chemistry* 22 (2008): 249–252.

79. D. Polidoro, T. Chhabra, E. Rodríguez-Castellón, et al., "Pd-N-Doped Carbons for Chemoselective Hydrogenation of Cinnamaldehyde: Unravelling the Influence of Particle Size and Support in Multiphase Batch and Continuous-Flow Systems," *Applied Catalysis A: General* 685 (2024): 119864.

80. C. He, J. Ke, H. Xu, and A. Lei, "Synergistic Catalysis in the Sonogashira Coupling Reaction: Quantitative Kinetic Investigation of Transmetalation," *Angewandte Chemie* 125 (2013): 1567–1570.

81. Y. Wu, X. Huo, and W. Zhang, "Synergistic Pd/Cu Catalysis in Organic Synthesis," *Chemistry - A European Journal* 26 (2020): 4895–4916.

82. Y. Huang, J. Huang, Y. Zhou, X. Fan, and Y. Li, "Pd@HKUST-1@Cu(II)/CMC Composite Bead as an Efficient Synergistic Bimetallic Catalyst for Sonogashira Cross-Coupling Reactions," *Carbohydrate Polymers* 324 (2024): 121531.

83. K. A. Goulas, S. Sreekumar, Y. Song, et al., "Synergistic Effects in Bimetallic Palladium–Copper Catalysts Improve Selectivity in Oxygenate Coupling Reactions," *Journal of the American Chemical Society* 138 (2016): 6805–6812.

84. I. P. Beletskaya and A. V. Cheprakov, "The Complementary Competitors: Palladium and Copper in C–N Cross-Coupling Reactions," *Organometallics* 31 (2012): 7753–7808.

85. Y. Q. Zhang, N. Kepčija, M. Kleinschrodt, et al., "Homo-Coupling of Terminal Alkynes on a Noble Metal Surface," *Nature Communications* 3 (2012): 1–8.

86. W. Shi and A. Lei, "1,3-Diyne Chemistry: Synthesis and Derivations," *Tetrahedron Letters* 55 (2014): 2763–2772.

87. C. M. Storey, M. Atthew, R. Gyton, et al., "Terminal Alkyne Coupling Reactions through a Ring: Mechanistic Insights and Regiochemical Switching," *Angewandte Chemie* 130 (2018): 12179–12182.

88. B. M. Trost and J. T. Masters, "Transition Metal-Catalyzed Couplings of Alkynes to 1,3-Enynes: Modern Methods and Synthetic Applications," *Chemical Society Reviews* 45 (2016): 2212–2238.

89. Y. Zhou and J. Zhao, "Glaser Coupling- and Sonogashira Coupling-Control over Cu_xO Nanoparticles/Carbon Nanotube by Switching Visible-Light Off and On," *Applied Catalysis B: Environmental* 300 (2022): 120721.

90. M. H. Vilhelmsen, J. Jensen, C. G. Tortzen, and M. B. Nielsen, "The Glaser–Hay Reaction: Optimization and Scope Based on ^{13}C NMR Kinetics Experiments," *European Journal of Organic Chemistry* 2013 (2013): 701–711.

Supporting Information

Additional supporting information can be found online in the Supporting Information section. **Supporting Scheme S1:** Schematic representation of possible products formed by substrate scope of Table S2. **Supporting Fig. S1:** N_2-physisorption of 5%Pd/CN^e material. **Supporting Fig. S2:** High resolution XPS spectra of 1%Pd/C-N^e (A-D), 5%Pd/C-N^e (E-H), 5%Cu/C-N^e (I-L) and 5%PdCu/C-Ne (M-Q). C 1s regions (A, E, I, M); N 1*s* regions (B, F, J, N); O 1s regions (C, G, K, O); Pd 3*d* regions (D, H, Q); Cu 2*p* regions (L, P). **Supporting Fig. S3:** Representative HRTEM image of the5%Pd/CN^e material. For more details, full characterization can be found in [17]. **Supporting Fig. S4:** STEM and EDX-mapping micrographs of 1%Pd/C-N^e and 5%Cu/C-N^e, with the corresponding Pd and Cu nanoparticle size distribution. **Supporting Fig. S5:** Catalytic performance of the different materials, including the theoretical activity. **Supporting Fig. S6:** Time-dependent profiles of the Sonogashira coupling and the phenylacetylene dimerization under mechanochemical extrusion. Sonogashira: Iodobenzene (5 mmol), phenylacetylene (1.5 eq.), K_2CO_3 (3 eq.), 5%PdCu/C-N^e (120 mg), 115°C, 100 rpm. Phenylacetylene dimerization: Phenylacetylene (7.5 mmol), K_2CO_3 (3 eq.), 1%Pd/C-N^e (100 mg), 100°C, 100 rpm. **Supporting Fig. S7:** Different dispersion of commercial carbon (left) and nitrogen-doped carbon derived from shrimp shells (right). **Supporting Fig. S8:** Mass spectrum (EI, 70 eV) of phenylacetylene. **Supporting Fig. S9:** Mass spectrum (EI, 70 eV) of iodobenzene. **Supporting Fig. S10:** Mass spectrum (EI, 70 eV) of Bromobenzene. **Supporting Fig. S11:** Mass spectrum (EI, 70 eV) of 3-Bromotoluene. **Supporting Fig. S12:** Mass spectrum (EI, 70 eV) of 4-Chlorotoluene. **Supporting Fig. S13:** Mass spectrum (EI, 70 eV) of 4-Iodoanisole. **Supporting Fig. S14:** Mass spectrum (EI, 70 eV) of 4-Iodoacetophenone. **Supporting Fig. S15:** Mass spectrum (EI, 70 eV) of Diphenylacetylene (product 1). **Supporting Fig. S16:** Mass spectrum (EI, 70 eV) of Triphenylethylene. **Supporting Fig. S17:** Mass spectrum (EI, 70 eV) of ((1*E*)-1,4-diphenylbut-1-en-3-yn-2-yl)benzene (product 2). **Supporting Fig. S18:** Mass spectrum (EI, 70 eV) of Biphenyl (product 3). **Supporting Fig. S19:** Mass spectrum (EI, 70 eV) of 1,4-diphenylbutadyine (product 4). **Supporting Fig. S20:** Mass spectrum (EI, 70 eV) of ((1*E*)-4-phenylbut-1-en-3-yn-1-yl)benzene (product 5). **Supporting Fig. S21:** Mass spectrum (EI, 70 eV) of 1,2,4-Triphenylbenzene. **Supporting Fig. S22:** Mass spectrum (EI, 70 eV) of 1-methyl-3-(phenylethynyl)benzene. **Supporting Fig. S23:** Mass spectrum (EI, 70 eV) of 1-methoxy-4-(phenylethynyl)benzene. **Supporting Fig. S24:** Mass spectrum (EI, 70 eV) of 1-(4-(phenylethynyl) phenyl)ethenone. **Supporting Fig. S25:** Mass spectrum (EI, 70 eV) of 3-phenylprop-2-yn-1-ol. **Supporting Fig. S26:** Mass spectrum (EI, 70 eV) of 1-methyl-3-(3-methylphenyl)benzene. **Supporting Fig. S27:** ^1H NMR (600 MHz, $CDCl_3$, 298 K) of diphenylacetylene (product 1). **Supporting Fig. S28:** ^1H NMR (600 MHz, $CDCl_3$, 298 K) of 1,4-diphenylbutadyine (product 4). **Supporting Fig. S29:** ^{13}C NMR (600 MHz, $CDCl_3$, 298 K) of diphenylacetylene (product 1). **Supporting Fig. S30:** ^{13}C NMR (600 MHz, $CDCl_3$, 298 K) of 1,4-diphenylbutadyine (product 4). **Supporting Table S1:** Textural properties of all materials mentioned in this work. **Supporting Table S2:** Substrate scope of Sonogashira cross-coupling reaction under solvent-free mechanochemical conditions. Aryl halide (5 mmol), Alkyne (1.5 eq.), K_2CO_3 (3 eq.), 5%PdCu/C-N^e (90 mg), 115°C, 1 h, 100 rpm.